Scour variability across offshore wind farms (OWFs): Identifying 1 site-specific scour drivers as a step towards assessing potential 2 impacts on the marine environment 3 4 5 Karen Garcia^{1*}, Christian Jordan¹, Gregor Melling³, Alexander Schendel^{1,2}, Mario Welzel¹, Torsten 6 Schlurmann^{1,2} 7 ¹Leibniz University Hannover, Ludwig-Franzius-Institute for Hydraulic, Estuarine and Coastal Engineering, 8 Nienburger Str. 4, 30167 Hannover, Germany. Email: schendel@lufi.uni-hannover.de, jordan@lufi.uni-9 hannover.de, welzel@lufi.uni-hannover.de, schlurmann@lufi.uni-hannover.de 10 ²Coastal Research Centre, Leibniz University Hannover & Technical University Braunschweig, Merkurstraße 11 11, 30419 Hannover, Germany. 12 ³ Federal Waterways Engineering and Research Institute (BAW), Wedeler Landstraße 157, 22559 Hamburg, 13 Germany. Email: gregor.melling@baw.de 14 *Corresponding author: garcia@lufi.uni-hannover.de Abstract: The development of offshore wind farms (OWFs) is critical to meeting renewable energy targets, but 15 predicting scour around offshore wind energy structures (OWES) and the associated potential impacts on marine 17 ecosystems remains a challenge. Using high-resolution bathymetry data, this study analyses field-measured scour 18 depth at 460 monopiles at nine British OWFs. The analysis reveals a large spatial variability of relative scour depth 19 (S/D) between OWF sites, but also within individual wind farms. Principal component analysis (PCA) is used to identify significant drivers of this variability. When the entire data set is considered, results indicate that the relative 20 water depth (h/D), the relative median grain size (D/d_{50}) , Keulegan-Carpenter number (KC_{99}) , and the sediment mobility parameter MOB (θ_{99}/θ_{m}) are the most important influencing factors for the variability of relative scour 23 depth. Other parameters investigated, such as pile Reynolds number (Re99), flow intensity $(U_{II})_{99}$, and Froude number (Fr_{99}) , were found to have a less clear influence. Further sediment-specific analysis shows that relative water depth (h/D) is a particularly relevant driver of scour at sites with fine $(63 \le d_{50} < 200$ 26 μm) and medium sands (200 $\leq d_{50} <$ 630 μm), with larger relative scour depth occurring in shallower relative 27 water depth. 28 Findings from this study provide new insights into scour behavior across a range of spatial and environmental scales and lay a foundation for the transferability of scour prediction frameworks to new OWF sites. In the future, findings and datasets from this study are suggested to be used to estimate scour-induced sediment transport and thereby to provide a step towards the assessment of potential impacts of OWF expansion scenarios in the marine 31 environment. By addressing the broader implications for regional sediment dynamics, this research contributes to 33 the sustainable development of offshore wind energy. 34 35 Keywords: Offshore wind farms (OWFs), relative scour depth, monopile, sediment transport, principal component analysis (PCA).

37 1 Introduction & Motivation

The expansion of renewable energy is crucial for a sustainable and independent energy supply. In order to meet the European Union's targets for expanding offshore wind energy (EU, 2020), it is necessary to develop areas with 40 previously unveiled metoceanic and geophysical conditions. To this end, existing knowledge gaps about the interaction of individual offshore wind energy structures (OWES) or entire offshore wind farms (OWFs) with the 41 marine environment must be closed. In general, the disturbance of the flow by an offshore structure causes scour, 42 43 which might not only affect the structure's stability (Saathoff et al., 2024), but the mobilized sediment may also contribute to the overall regional sediment transport (Vanhellemont et al., 2014; Baeye and Fettweis, 2015; Rivier 44 45 et al., 2016) with potential impacts on the marine environment. The scour process itself, is a multivariate process, which is dependent on a combination of complex hydrodynamic 47 and geotechnical drivers. Early studies focused on the understanding of the scour process around a pile under 48 simplified isolated hydraulic conditions, such as steady flow (e.g., Sheppard et al., 2004; Zhao et al., 2012; Sarkar 49 et al., 2014; Baykal et al., 2015), unsteady and bidirectional tidal currents (e.g. Escarameia and May1999; McGovern et al., 2014; Yao et al., 2016; Schendel et al., 2018) and waves (e.g. Sumer et al., 1992b; Carreiras et 50 al., 2001; Stahlmann et al., 2013). With the availability of more sophisticated experimental facilities and numerical 51 52 models, research is increasingly shifting toward more complex hydrodynamic loads consisting of a combination of waves and currents, as in the studies of Sumer and Fredsøe (2001), Qi and Gao (2014), Schendel et al. (2020), 53 Lyu et al. (2021), and Du et al. (2022) and also towards studies addressing complex offshore structures (Welzel, 55 2021; Welzel et al., 2024; Sarmiento et al., 2024; Chen et al., 2025). 56 Despite those advances in scour research, uncertainties remain in current scour prediction methods (Chen et al., 2024). Matutano et al. (2013) demonstrated the challenges of applying empirical formulas for maximum scour 57 58 depth by comparing different methods with data from ten European OWFs, revealing overpredictions in all but two cases. The comparison highlights the fundamental challenge of accounting for complex marine flow 59 conditions, characterized by the combined effect of multiple influencing factors, such as flow velocity, sediment 60 coarseness, and wave-current interactions, in the prediction of scour processes using existing models (Gazi et al., 2020; Harris et al., 2023). Compared to laboratory experiments focusing on scour processes, rather few studies are 62 based on in-situ data, that represent the actual scour development under complex flow conditions. These studies 63 assessed the scour at individual structures, such as monopiles (Walker, 1995; Noormets et al., 2003; Harris et al., 64 2004; Rudolph et al., 2004; Louwersheimer et al., 2009), and jackets (Bolle et al., 2012; Baelus et al., 2018), or 65 dealt with larger datasets from entire offshore wind projects (DECC 2008; COWRIE 2010; Whitehouse et al., 66 67 2010; Whitehouse et al., 2011; Melling (2015)), covering both spatial and temporal evolution of scour under 68 different hydrodynamic regimes and seabed types across the North Sea and British continental shelf. In general, the amount and variety of field data collected has increased with the gradual installation of OWES. 69 70 Focusing specifically on the correlation between scour and on-site conditions, Melling (2015) analyzed the relationships between the variations of scour hole dimension within OWFs and both sedimentological and 71 72 hydrodynamic parameters of 281 OWES in the Outer Thames estuary. Melling's (2015) study, although only 73 covering three OWFs, represents one of the most comprehensive investigations of field related scour to date, with the highest number of structures examined so far. By comparing field data with physical modeling experiments 74 and literature, the study provided valuable insights into the range of observed scour and its controlling structural hydrodynamic, and sedimentological parameters.

In addition to local scour at individual structures, the cumulative effect of multiple structures in an OWFs can alter 77 ocean dynamics (Christiansen et al., 2022), mixing (Schultze et al., 2020), and sediment mobility, resulting in 78 79 changes to suspended sediment concentrations and wave-induced turbidity plumes (Vanhellemont & Ruddick, 2014). This can also lead to dynamic interactions with migrating seabed features, such as sand waves (Matthieu & 80 81 Raaijmakers, 2012). Increased velocities and turbulence induced by OWFs has also the potential to affect the 82 marine environment, potentially leading to global erosion around the structures as well as habitat loss or gain for 83 benthic flora and fauna (Shields et al., 2011; Wilson and Elliott, 2009; Welzel et al., 2019). Concerns over the 84 potential impacts of OWF installations on local ecosystems further include collision risks, noise pollution, 85 electromagnetic field and the introduction of invasive species (Lloret et al., 2022; Bailey et al., 2014; Teilmann 86 and Carstensen, 2012; Watson et al., 2024). As the size and scale of OWF increases, the risk of significant cumulative effects arising is also expected to increase (Brignon et al., 2022; Gusatu et al., 2021). The drivers and 87 interdependencies of these large-scale processes are not yet well understood and the precise impact of scour induced sediment transport on the marine environment remains uncertain, highlighting the need for 90 interdisciplinary research utilizing field data. In order to gain a better understanding of the geophysical changes following the installation of OWFs and potential impacts on the marine environment arising from it, this study analyses the scour development at OWES as a first 92 93 step. This study builds its analysis on field data, including high-resolution bathymetry scans from British OWFs, 94 which have recently been made publicly available. This provides an opportunity to extend the understanding of scour evolution and its key drivers using a cross-regional dataset. A total of 460 monopiles were analyzed to obtain local scour depth and their spatial distribution in dependence of selected hydrodynamic and geological drivers. 97 Understanding scour development is a critical first step in assessing potential environmental impacts. It will help 98 determine whether OWES and entire OWFs contribute to regional sediment mobilization and provide a foundation 99 for future research into the long-term morphological footprint of OWF installations and their broader ecological 100 effects. To contribute to the overarching goal of reducing uncertainty in scour predictions at OWES this study analyzes field data from 460 monopiles across 9 OWFs, situated in diverse ocean regimes with current velocities 101 102 from 0.54 m/s to 1.77 m/s (99th percentile), significant wave heights from 1.5 m to 2.7 m (99th percentile), water depths from 5 to 35 m and grain sizes ranging from cohesive sediment (51.54 μm) to medium gravel (19872 μm). 103 The spatial distribution and variability of relative scour depth across and within these OWFs are determined and 104 105 correlated with selected hydrodynamic and sedimentological parameters, using Principal Component Analysis 106 (PCA). This analysis aims to (1) identify universal drivers of scour across all sites, (2) assess sediment specific 107 trends by grain size (d_{50}) and (3) evaluate site specific variability at the level of three selected OWFs (Robin Rigg, 108 Lynn and Inner Dowsing and London Array). The site specific analysis in Section 3.5 assesses the robustness of 109 the global correlations under local conditions and provides insight into how local conditions influence scour 110 behavior. Collectively these efforts aim to decrease uncertainty in relative scour depth prediction by assessing the contribution of the main drivers of scour development from multivariable field data. 111 112 This paper is organized as follows: Section 2 describes the study area and methodology in which the methods used to obtain the relative scour depth and selected on-site parameters are explained in detail (subsections 2.2 - 2.5). 113 Additionally, the application of the PCA to identify the primary correlation between these parameters and scour 114 development is explained (subsection 2.6). The results are presented in section 3, followed by discussion (section 4) and ending with the conclusions (section 5).

117 2 Study area and methodology

118 2.1 Study area

- 119 The research area, located in British waters, is illustrated in Figure 1, showing the specific locations of the nine
- 120 studied OWFs. Figure 1A provides a general overview, while Figure 1B pinpoints the positions of the OWFs,
- 121 labeled 1 to 9. These OWFs correspond to Robin Rigg, Barrow, Teesside, Humber Gateway, Lincs, Lynn and
- 122 Inner Dowsing, Greater Gabbard, London Array, and Gunfleet Sands, respectively. Figures 1C and 1D display the
- 123 99th percentiles of the significant wave heights $(H_{s,99})$ and current velocity magnitudes (U_{99}) at the nine locations,
- 124 respectively.
- 125 Notably, wind farms such as Robin Rigg and Barrow are situated in the Irish Sea, while the remaining seven are
- 126 located in the North Sea at the east coast of UK (Fig 1B). Water depths (h) ranging from 5 to 35 m can be found
- 127 across the nine OWFs. Depth data (h) were obtained from EMODNET
- 128 (https://emodnet.ec.europa.eu/en/bathymetry). The OWF located in the shallowest water depth is Robin Rigg
- 29 with h ranging from 1 to 14 m (Fig. 1B). Conversely, the OWF with the deepest water depth is Greater Gabbard
- 130 with h ranging from 21 to 35 m (Fig. 1B).
- 131 The highest and lowest significant wave heights (99th percentile) can be found at Humber Gateway OWF ($H_s = 2.7$
- 132 m) (Fig. 1C-D) and at Gunfleet Sands OWF ($H_s = 1.5$ m), which are located at the mouths of the Humber and
- 133 Thames estuaries (Fig. 1C-D), respectively. Regarding current velocities, the highest value is found at Robin Rigg
- 134 OWF with 1.8 m/s (Fig. 1C-D), while the lowest value is found at Gunfleet Sands OWF with a value of 0.4 m/s
- 135 (Fig. 1C-D).
- 136 Depending on the locations of the OWFs, the seabed conditions vary from sandbanks featuring a variety of
- 137 bedforms to intertidal mudflats. Accordingly, the sediment also varies from silt to coarse and very coarse gravel,
- 138 with the sediment at Teesside OWF consisting of fine and silty sands and that at Humber Gateway consisting of
- 139 sandy gravel and boulders. In contrast, OWFs such as London Array and Greater Gabbard are located in the Outer
- 140 Thames Estuary with sandbanks and channels, while others such as Barrow and Robin Rigg have distinct
- 141 geological features such as megaripples, mudflats and deposits from different geological eras.

143 2.2 Data description

- 144 Bathymetric datasets from the nine OWFs considered in this study were collected via multibeam echosounder
- 145 (MBES) before, during and after the construction of the OWFs and were afterwards made available by its operators
- 146 via the Marine Data Exchange (MDE).
- 147 In total 460 OWES (of 680 available) with monopiles foundations were analyzed in this study. For the correlation
- 148 between scour and hydrodynamic conditions at the nine studied OWFs, metocean hindcast datasets (i.e., significant
- 149 wave height (H_s) and velocity magnitude (U)) by the Copernicus Marine Service (CMEMS)
- 150 (https://marine.copernicus.eu/) were used (CMEMS, 2023a, 2023b).

151

142

152

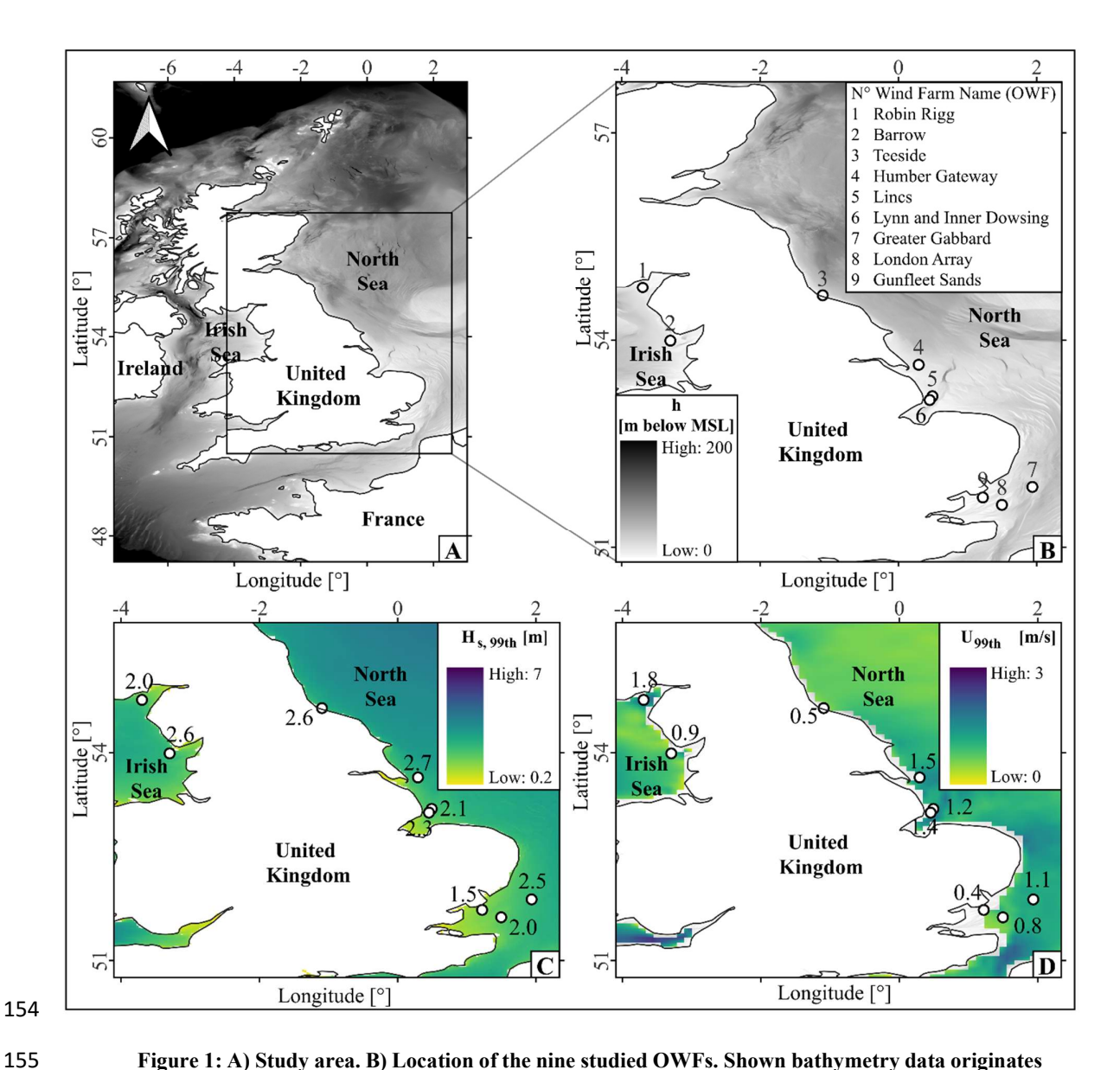


Figure 1: A) Study area. B) Location of the nine studied OWFs. Shown bathymetry data originates from EMODET (https://emodnet.ec.europa.eu/en/bathymetry). C) 99th percentile of significant wave heights (H_s) based on data for the year 2012. D) 99th percentile of current velocity magnitudes (U) based on data for the year 2012.

Table 1 shows the OWFs considered in this study and provides an overview of their structural characteristics as well as the hydrodynamic and geotechnical site conditions. Pile diameters (D) were obtained from Negro et al. (2017), water depths (h) are based on EMODET (2020), d_{50} represents the median grain diameter of the sediment. The sediment data shown in Table 1 were obtained in Phi units from each OWF's benthic reports, then converted to d_{50} values in micrometers (μm) according to Bunte et al. (2001). The scour depth S represents the deepest scour at an individual OWES. The number of OWES varies from 26 OWES installed at Teesside OWF to 174 OWES installed at London Array OWF, indicating the different operational scales. For some OWFs, including Lynn and Inner Dowsing, extensive bathymetric data spanning over ten years was available. In contrast, others, such as Humber Gateway, had more limited bathymetric data with a coverage duration of four years. The highest grid resolutions of the bathymetric datasets found at each OWF varied from 0.2 to 0.5 m, with the highest resolution

of the bathymetries found at each OWF being used. The earliest bathymetry was collected at Barrow OWF in 2005 169 and the most recent was collected at Lynn and Inner Dowsing in 2017, highlighting the long-term monitoring 170 efforts at the wind farms. However, in this study only scour depth obtained from the pre- and the first post-171 construction bathymetries were considered. The shortest period between pre and post bathymetries was found at Lincs OWF with 377 days between August 2010 and August 2011, while the longest period between scans was 173 174 detected at Greater Gabbard OWF with 2902 days (~8 yrs) between June 2005 and May 2013. 175 Furthermore, environmental and hydrodynamic conditions associated with each OWF are also shown in Table 1, which are essential for understanding how different variables contribute to scour around monopiles. These 176 177 variables include the 99th percentile significant wave height ($H_{s,99}$), representing the average height of the highest third of waves. The wave height has a direct influence on the wave-induced current velocity near the seabed and 178 179 thus strongly determines the bed shear stresses and the formation of the vortex system around the OWES (Sumer & Fredsøe, 2002; Schendel et al., 2018). The 99th percentile current velocity magnitude (U_{99}) indicates the resultant 180 of eastward (u_0) and northward (v_0) tidal flow components, those represent the depth-average velocity magnitude, 181 whereas U_{cr} depicts the critical flow velocity for sediment entrainment. Their ratio, the flow intensity $(U_{/I_{cr}})_{99}$ 182 183 is a key parameter in describing the general sediment mobility and has a large impact (h/D) influences the 184 formation of the horseshoe vortex in such a way that the size of the horseshoe vortex is reduced as the flow depth decreases, resulting in a reduction in the relative scour depth. At greater relative water depth $h/D \ge 5$) the relative 185 186 scour depth becomes almost independent of relative water depth (Sumer and Fredsøe, 2002). 187 The Froude number (Fr_{99}) and pile Reynolds number (Re_{99}) are used to characterize the flow conditions around 188 the pile and their calculations are shown in table 2, Equations 2 and 3. The Froude number indicates whether the flow is dominated by gravitational or inertial forces. With increasing Froude number, stronger inertial forces 189 190 produce more pronounced pressure gradients at the upstream face of the monopile. Promoting early boundary layer 191 separation and enhances the strength of the horseshoe vortex system near the seabed, which increases local bed 192 shear stress and accelerates sediment erosion. As shown by Hu (2021), these dynamics are key in amplifying scour. 193 Similarly, Corvaro et al. (2015) found that higher Froude numbers lead to larger vortex structures and increased 194 bed shear stress, resulting in deeper equilibrium scour depth. On the other hand, the Reynolds numbers provides 195 information on whether the flow is laminar or turbulent, and determines the characteristics of the vortex system 196 around the pile. 197 Additionally, the Keulegan-Carpenter number (KC_{99}) , which is used to determine the relative influence of drag and inertia forces, the formation of vortices, and the potential for sediment transport (Sumer & Fredsøe, 2002). 198 The mobility parameter $(\theta_{99}/\theta_{rr})$ is considered a key controlling factor for scour, as it reflects the onset of sediment 199 200 motion under given flow conditions (Soulsby, 1997; Whitehouse et al., 2000). The calculation of those two parameters are shown in table 2, equation 9 and 20. The datasets were obtained between pre- and post- construction 201 bathymetries. The data was collected over a one-year period, prior to the post-construction bathymetry." 202 203 Dimensionless parameters as given in Table 1 were calculated based on the equations summarized in Table 2. 204

OWF name	N° of OWES	Pile diameter D (m)		Scour depth S (m)	Water depth h (m)	D ₅₀ (μm)	Wave height $H_{s,99}$ (m)	Current Velocity U_{99} (m/s)	Relative scour depth S/D	Relative water depth h/D	Froude number Fr_{99}	Reynolds number Re ₉₉	Keulegan Carpenter number <i>KC</i> ₉₉	Mobility parameter θ_{99}/θ_{cr}	Flow intensity $(U/U_{cr})_{99}$
Robin Rigg	60	4.3	Min Max	1.3 10	5 14	167 267	2.36 2.59	1.55 1.77	0.30 2.32	1.03 3.07	0.13 0.23	5.14x10 ⁶ 5.86x10 ⁶	0.99 1.9	15.3 25.4	3.51 4.43
Barrow	30	4.75	Min Max	0.98 6	15 23	138 445	2.43 2.52	0.91 1.11	0.20 1.20	3.67 4.71	0.06 0.08	3.50x10 ⁶ 4.26x10 ⁶	0.34 0.48	4.4 7.2	1.89 2.40
Teesside	26	5	Min Max	0.65 1.62	8 20	51 166	2.52 2.76	0.54 0.54	0.13 0.32	208 3.49	0.04 0.05	2.10x10 ⁶ 2.10x10 ⁶	1.2 1.6	6.1 9.6	1.19 1.29
Humber Gateway	72	4.2	Min Max	0.5 2.51	15 20	5918 1900 0	2.24 2.37	1.51 1.56	0.11 0.59	3.65 4.65	0.11 0.12	4.87x10 ⁶ 5.06x10 ⁶	0.92 1.11	0.4 1.2	0.58 0.99
Lines	75	5.2	Min Max	0.54 1.92	12 21	505 1982	2.47 2.71	1.07 1.67	0.10 0.38	2.41 3.88	0.08 0.13	4.29x10 ⁶ 6.71x10 ⁶	0.64 1.01	2.6 11.1	1.31 3.12
Lynn and Inner Dowsing	60	4.74	Min Max	0.5 2.35	9 17	684 1950	2.11 2.36	1.30 1.45	0.10 0.49	2.10 3.47	0.11 0.13	4.76x10 ⁶ 5.29x10 ⁶	0.84 1.3	3.2 7.3	1.63 2.53
Greater Gabbard	139	6	Min Max	0.5 4.54	23 35	394 2296	2.41 2.67	1.02 1.22	0.08 0.75	3.50 5.83	0.05 0.07	4.72x10 ⁶ 5.64x10 ⁶	0.18 0.33	1.3 6.1	1.14 2.25
London Array	174	7	Min Max	1.2 9.5	1 27	120 930	1.89 2.36	0.71 0.81	0.21 2.02	0.31 4.67	0.04 0.19	$2.56 \times 10^6 \\ 3.56 \times 10^6$	0.1 2.3	1.5 32.6	1.14 2.33
Gunfleet Sands	49	4.7	Min Max	0.88 7.73	2 16	146 253	1.52 1.72	0.48 0.86	0.18 1.64	0.54 3.34	0.03	1.74x10 ⁶ 3.12x10 ⁶	0.45 1.68	2.1 17.6	1.05 2.07

Table 1. Overview of studied OWFs with hydrodynamic and sedimentological site conditions.

211 Table 2. Calculation of the variables included in the analysis

Variable	Equation	
Current velocity	$U_{99} = \sqrt{u_0^2 + v_0^2}$	(1)
Froude number	$Fr_{99} = rac{U}{\sqrt{gh}}$	(2)
Pile Reynolds number	$Re_{99} = \frac{U D}{v}$	(3)
Dimensionless grain size	$D_* = \left(\frac{\rho g}{v^2}\right)^{\frac{1}{3}} d_{50}$	(4)
Critical Shields	$\theta_{cr} = \frac{0.3}{1 + 1.2D_*} + 0.55(1 - \exp(-0.02D_*)$	(5)
U_{cr}	$U_{cr} = 7 * \left(\frac{h}{d_{50}}\right)^{\frac{1}{7}} (g(s-1)d_{50}\theta_{cr})^{0.5}$	(6)
Flow intensity	$(\frac{U}{U_{cr}})_{99}$	(7)
Zero crossing period (T_z)	$\frac{T_p}{1.28}$	(8a)
Natural period (T_n)	$T_n = \sqrt{\frac{h}{g}}$	(8b)
A_{t}	$A_t = \left(6500 + \left(0.56 + 15.54 \frac{T_n}{T_z}\right)^6\right)^{1/6}$	(8c)
RMS velocity (U _{rms})	$A_{t} = (6500 + \left(0.56 + 15.54 \frac{T_{n}}{T_{z}}\right)^{6})^{1/6}$ $U_{rms} = 0.25 \frac{H}{T_{n}(1 + \left(A_{t} \frac{T_{n}^{2}}{T_{z}}\right))^{3}}$	(8d)
Wave-induced velocity (U_m)	$U_m = \sqrt{2} \ U_{rms}$	(8e)
Keulegan-Carpenter number (KC)	$KC_{99} = \frac{U_m T_p}{D}$	(9)
Roughness related to d_{50} (ks)	$k_s = 2.5d_{50}$	(10)
Amplitud of wave orbital motion at the bed (<i>A</i>)	$A = \frac{U_m T_p}{2\pi}$	(11)
shear velocity (U_f)	$A = \frac{U_m T_p}{2\pi}$ $U_f = \frac{U}{6.0 + 2.5 \ln\left(\frac{h}{k_s}\right)}$	(12)

$$f_{w} = \begin{cases} 0.32 \left(\frac{A}{k_{s}}\right)^{-0.8}, & \frac{A}{k_{s}} < 2.92 \end{cases} \\ 0.237 \left(\frac{A}{k_{s}}\right)^{-0.52}, 2.92 \leq \frac{A}{k_{s}} < 727 \\ 0.04 \left(\frac{A}{k_{s}}\right)^{-0.25}, & \frac{A}{k_{s}} \geq 727 \end{cases} \\ \text{angular difference} \\ \text{between the direction of the wave and the current} \\ (\alpha) \\ \text{current induced bed shear stress} (\tau_{c}) \\ \text{the wave induced bed shear stress} (\tau_{w}) \\ \text{cycle-mean shear stress} (\tau_{m}) \\ \text{cycle-mean shear stress} (\tau_{m}) \\ \text{the to a combined wave-current load} \\ \text{maximum shear stress} \\ \text{value under combined wave-current load} \\ \text{maximum shear stress} \\ \text{value under combined wave-current load} (\tau_{b}) \\ \text{Shields parameter} \\ \theta_{99} = \frac{\tau_{max}}{(\rho_{s} - \rho_{w})gd_{50}} \\ \theta_{99} = \frac{\tau_{max}}{(\rho_{s} - \rho_{w})gd_{50}} \\ (20) \\ \end{cases}$$

The values assumed for all OWFs sites are:

213 $\rho_s = 2650 \, kg/m^3, \, \rho_w = 1027 \, kg/m^3, \, v = 1.3x10^{-6} m^2/s, \, g = 9.8 \, m/s^2$

Where ρ_s is the sediment density, based on Soulsby (1997). ρ_w is the water density, v is the kinematic viscosity and g the gravitational acceleration. Equation 4 was calculated based on van Rijn (1984), where D_* is the non-dimensional grain diameter that is used to calculate the critical Shields parameter (θ_{cr}), which represents the threshold for initiation of motion at the bed, as proposed by Soulsby (1997).

Equation 5 is taken from Soulsby and Whitehouse (1997), where s ($s = {\rho_s}/{\rho_w}$) represents the specific gravity of sediment grains. The d_{50} represents the median sediment grain size.

In equation 18, the maximum bed shear stress value (τ_{max}) was calculated following Roulund et al. (2016), which builds upon Soulsby (1997) by combining current- and wave-induced shear stress through a directional correction. Shields parameter (θ_{99}) is derived using equation 19, based on the maximum bed shear stress (τ_{max}) under combined wave and current conditions. The Keulegan–Carpenter number is defined in equation 10, where T_p is the peak wave period and D the monopile diameter.

Equation 20 provides the calculation of the mobility parameter to assess sediment mobility, providing a dimensionless indicator of whether the hydrodynamic forcing was sufficient to initiate sediment motion. All relevant equations are summarized in table 2.

229 2.3 Pre-processing of bathymetric data

225

226227

228

230

231

232

Figure 2 shows the workflow used in this study, starting with the acquisition of bathymetric datasets, originally obtained from the Marine Data Exchange, and their conversion to Ordnance Datum Newlyn (ODN). This was followed by the generation of 100m x 100m tiles for each available bathymetric dataset, centered on each turbine location. If bathymetric scans with different spatial resolutions were available for the same date, only the one with

234 the highest resolution was used. In addition, some turbine locations could not be further analysed due to missing 235 pre-construction scans or poor data quality. Tiles with more than 50% empty cells were discarded because a high 236 percentage of missing data increases the likelihood that important areas, such as the scour region, are poorly 237 captured. Tests were conducted with lower missing cell thresholds (10% and 25%), but even with 50% missing data, valuable information for scour analysis was retained. Using a stricter 25% threshold, too many tiles were 238 239 lost, including those that still contained useful data. As a result, 460 OWES across the nine OWFs were analyzed 240 in this study. 241 The difference in bed elevation at turbine sites between the pre-construction (Fig 2.A) and post-construction 242 surveys (Fig 2.B), was used for extracting scour information. The deepest scour at each turbine site was then extracted from the difference plot (Figure 2.C). A detailed description of this part of the workflow is provided in 243 section 2.4. 244

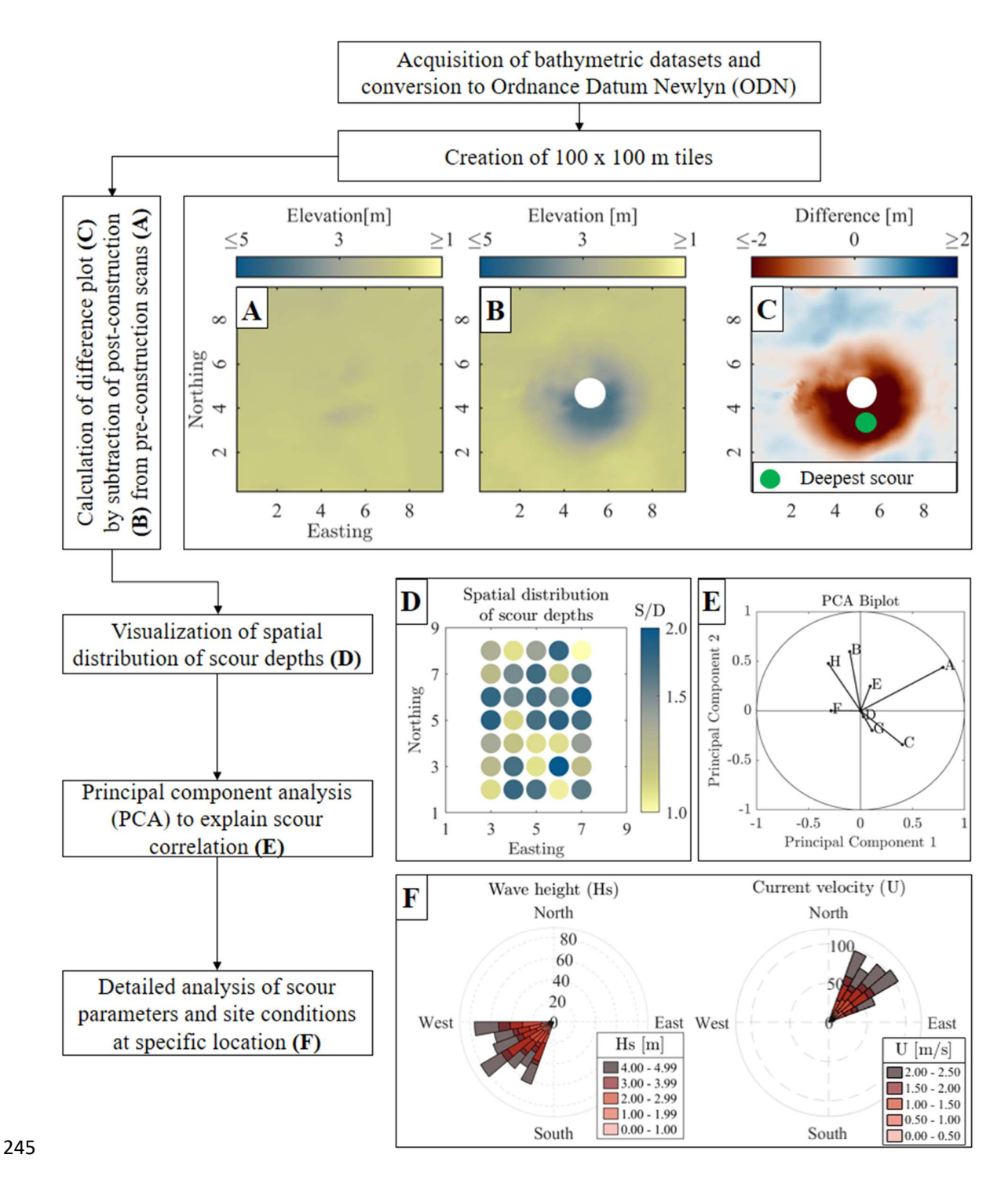


Figure 2: General workflow and methodology used to assess the scour distribution and evolution as well as the correlation between scour parameters and site conditions. A) Pre-installation scan. B) Post-installation scan. C) Difference plot after subtraction of B from -A. D) Map of spatial distribution of relative scour depth. E) Principal Component Analysis (PCA). F) Site conditions of wave heights and current velocities.

250 2.4 Calculation of scour parameters

246

247248

249

First, to eliminate outliers, a threshold based on the 99th percentile was used to filter out extreme values, ensuring that outliers did not skew subsequent analyses or visualizations. Subsequently, to address potential offsets between

- 253 pre- and post-construction, a median filter was applied to both datasets. The difference in medians, excluding the
- 254 presumed scour area, was considered the offset. This offset was then applied while calculating the difference plot
- 255 between the pre- and post-construction bathymetries (Fig. 2A-C). To remove additional outliers close to the
- 256 turbine, an area equivalent to 110% of the pile's footprint area was excluded from the center of the difference plot.
- 257 The deepest scour depth (see green dot in Fig. 2C) was then extracted from the difference plot (Fig. 2C). The
- 258 calculated relative scour depth were then visualized to show the spatial distribution across the nine OWFs (Fig.
- 259 2D).

260 2.5 Principal component analysis (PCA)

- 261 In the case of field data, the correlation of the scour process with hydrodynamic and geotechnical variables is
- 262 complicated by the simultaneous change of several of these variables. In order to reduce the complexity and
- 263 simplify this multivariate problem, PCA was used in a next step (Fig. 2.E). PCA works by transforming the data
- 264 into a set of new variables called principal components, which are linear combinations of the original variables
- 265 (Jolliffe & Cadima, 2016). These components are ordered based on how much variance they explain, with the first
- 266 principal component (PC1) explaining the maximum variance in the data, followed by the second principal
- 267 component (PC2). Each component also has an eigenvalue, which shows the amount of variation it captures.
- 268 Generally, the PCA is able to handle lots of independent variables and helps to simplify the data without losing
- 269 important information (Harasti, 2022).
- 270 In this study, the PCA was applied to a dataset of 692 OWES, including 460 from our analysis and an additional
- 271 232 OWES from London Array and Thanet OWF, based on Melling's (2015) data. The PCA was then performed
- 272 using eight independent variables that contributed to the principal components. Those dimensionless variables
- 273 were the relative water depth (h/D), Keulegan-Carpenter number (KC_{99}) , mobility parameter $(\theta_{99}/\theta_{cr})$, Reynolds
- 274 number (Re_{99}) , Froude number (Fr_{99}) , relative sediment size (D/d_{50}) , flow intensity $((U/U_{co})_{99})$, and the relative
- 275 scour depth (S/D). Following this, the data was organized into a matrix, with each row representing a specific
- 276 OWES and each column representing a selected dimensionless variable. All the variables were extracted as
- 277 representative values specific to the OWES, with the focus on the 99th percentile to capture extreme hydrodynamic
- 278 conditions. Scour processes are more likely to occur in these extreme conditions because maximum scour depth
- 279 usually develops during storm-induced events, rather than under mean or median values. Subsequently, the
- 280 variables were standarized to ensure the comparability of the results.
- 281 In some studies, the PCA is used for reducing the number of dimensions (Harasti, 2022), or to help develop
- 282 predictive models grouped by soil classes (Annad, 2023). However, the aim of this study was to keep all the
- 283 principal components. This approach enabled the full exploration of the interdependence between physical drivers
- and scour response across sites. To interpret the relationships among the variables, a principal component analysis
- 285 biplot was generated (Gabriel et al., 1971). In the biplot, variables are represented as vectors, and the angle between
- 286 vectors indicates the degree of correlation. The strength of the correlation was quantified using the cosine of the
- angle (Jolliffe & Cadima, 2016), enabling us to assess the strength of association between each variable and scour
- 288 variability across different OWFs sites. Similar to previous studies that applied PCA for parameter selection in
- 289 bridge pier or scour formula development (Harasti, 2022; Annad, 2023), this multivariate analysis provides a
- 290 clearer understanding of which parameters dominate the scour process under real offshore conditions

- An additional approach to reducing the complexity of multivariate datasets is to initially group the data based on a selected key variable. Accordingly, the PCA was also applied to the dataset after it had been grouped by grain size (d_{50} diameter) classes (Annad et al., 2021), given that the sediment characteristics of the seabed play a significant role in local scour (Qi et al., 2016). This approach facilitated a more precise estimation of local scour, thereby reducing uncertainties related to sediment.
- 296 3 Results

97 3.1 Spatial distribution of relative scour depth

298 To illustrate the variability in relative scour depth between the nine studied OWFs and within single OWFs, Figure 3 shows the spatial distribution of relative scour depth. There are clear differences between OWFs in both the 299 300 magnitude and variability of relative scour depth. For example, at OWF Robin Rigg (Figure 3.A), the highest relative scour depth were identified, the values range from S/D=0.29 to S/D=2.49. This OWF is characterized by 301 302 fine and medium sands. In contrast, the smallest relative scour depth occurred at the OWF of Lynn and Inner Dowsing (Figure 3.F), with values from S/D=0.12 to S/D=0.92, which is possibly linked to coarse sands presented 303 at this site. Furthermore, the highest variability ($\sigma = 0.44$) in relative scour depth were detected at OWF London 304 305 Array (Figure 3.H) and Barrow (Figure 3.B), likely influenced by the complex seabed morphologies and sediment 306 compositions in these areas. On the other hand, the significant variability at London Array may be explained by 307 the presence of the Long Sand and Kentish Knock sandbank. This illustrates how different site characteristics can 308 result in various scour distributions, even within a single OWF. 309 The remaining OWFs showed relatively low relative scour depth and little spatial variability, even though site conditions were significantly different, as indicated by their seabed conditions from very fine sand for Teesside 310

(Figure 3.C) to coarse and very coarse gravel for Humber Gateway (Figure 3. D).

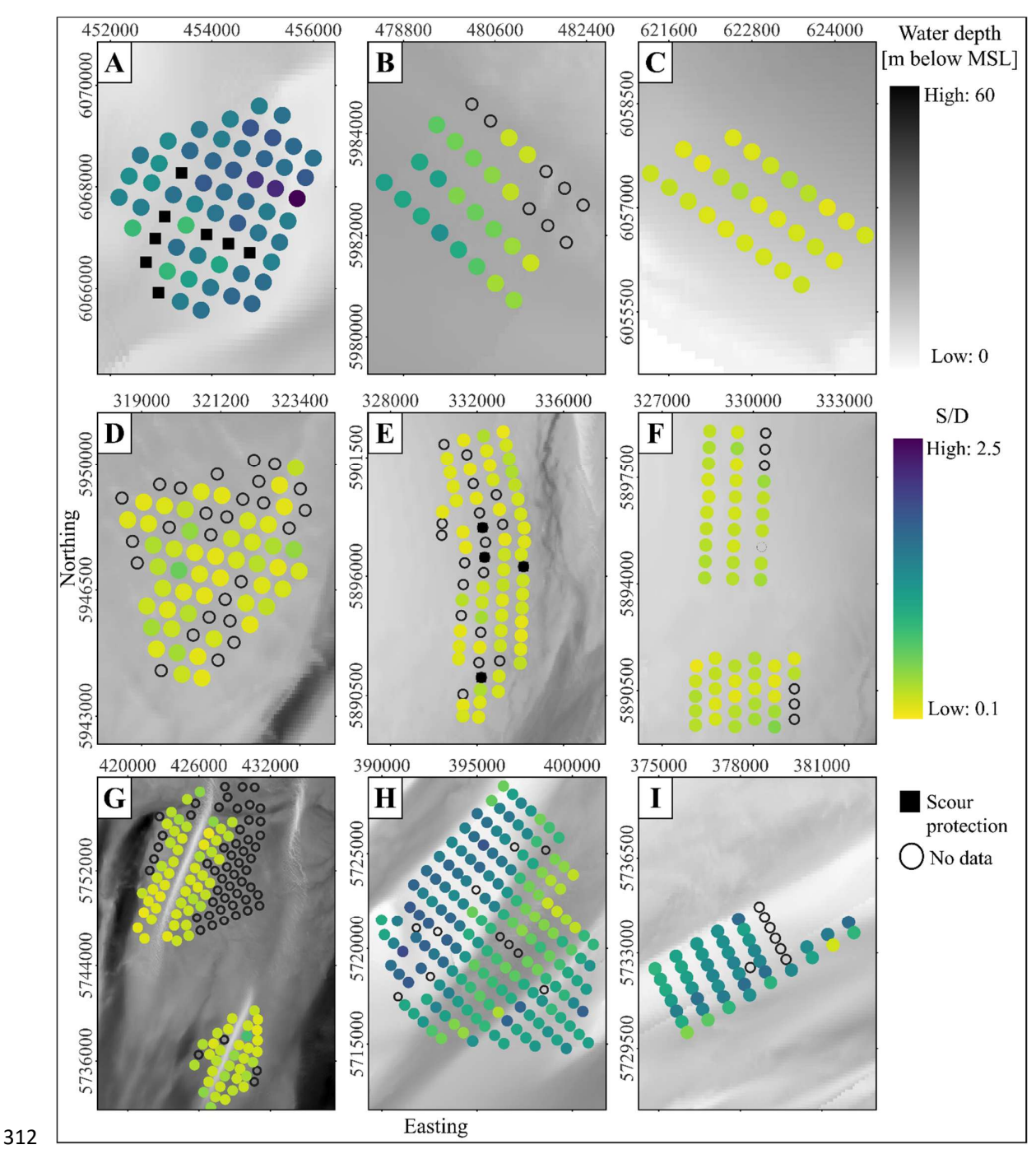


Figure 3: Spatial distribution of relative scour depth at the nine studied OWFs. Letterred markers (A-I) denote the locations of Robin Rigg, Barrow, Teesside, Humber Gateway, Lincs, Lynn and Inner Dowsing, Greater Gabbard, London Array, and Gunfleet Sands OWFs, respectively. The upper colorbar represents water depth, with darker shades indicating deeper water. The lower colormap indicates relative scour depth, with darker blue color indicating largest scour. Black filled squares represent OWES with scour protection, while empty circles denote missing data. Shown bathymetry data originates from EMODET (DEE).https://emodnet.ec.europa.eu/en/bathymetry).

320 3.2 Principal component analysis (PCA)

The analysis of Figure 3 reveals notable variations in relative scour depth across individual OWFs. This variance underscores the need for a more detailed examination of specific wind farm characteristics to identify the drivers of scour. To this end, a PCA was conducted to correlate relative scour depth and selected parameters by identifying and quantifying their relationships. The PCA biplot presented in Figure 4 illustrates these correlations between relative scour depth and the studied variables and provides a comprehensive view of how different factors interact and influence relative scour depth.

Cosinebased

Correlation

with S/D

0.96

0.81

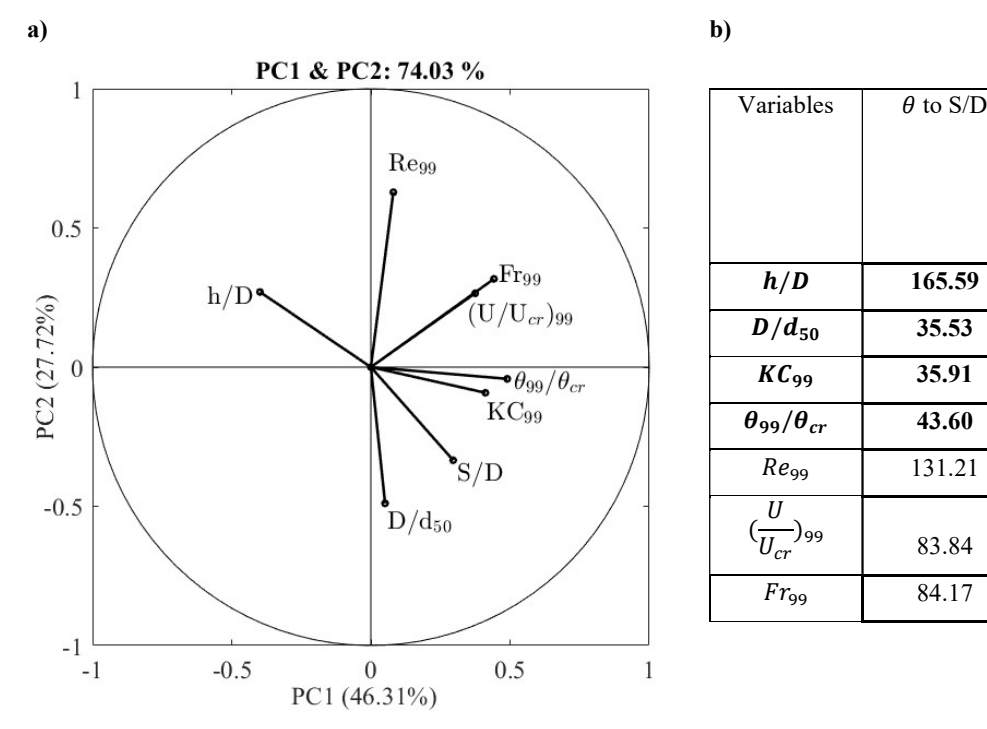
0.80

0.72

0.65

0.11

0.10



321 322

323

324 325

326

327328

329

330

331

332

333334

335

336337

338339

340

341342

343

344

Figure 4: a) PCA biplot, illustrating the correlation between variables and relative scour depth . b) The table detailing the angles between the relative scour depth and the other variables (in degrees), along with the magnitude cosine-based correlation (values from 0 to 1), where values closer to 1 indicates stronger correlation.

As shown in the biplot, PC1 and PC2 account for 74.03% of the variation in the data set. This high percentage indicates that these two components capture most of the significant patterns in the data, allowing for a meaningful interpretation of the relationships among the variables. In the biplot, each vector stands for a variable, with the direction and magnitude of the vector reflecting its contribution to the principal components. The variables that contribute the most to the variance in PC1 are the mobility parameter, the Froude number, and Keulegan Carpenter number, with shares of 0.4898, 0.4419, and 0.4114, respectively. In contrast, the variance in PC2 is primarily explained by the pile Reynolds number, the relative grain size and the Froude number, with shares of 0.628, - 0.489, and 0.3168, respectively. This significant contribution of the mobility parameter, the Froude number, and the Keulegan Carpenter number to PC1 suggests that variations in these hydrodynamic parameters are critical in shaping the principal dynamics of the dataset. The table (Fig. 4b) next to the biplot provides further insight by showing the angular distances between the *S/D* vector and each of the other variables, as well as their respective correlation coefficients. One of the key observations is that relative scour depth has the strongest negative correlation of 0.96 with the relative water depth, which underscores the critical role of water depth in governing scour intensity. Shallower relative depths concentrate flow energy at the bed, intensifying near-bed velocities and

shear stresses that promote deeper scour holes (Smith & McLean, 1977; Whitehouse, 2010). The next strongest 345 346 correlation is with the relative grain size with a correlation factor of 0.81. This suggests that as the relative grain size increases, relative scour depth also tends to increase. This trend is in line with the functional dependence of 347 relative scour depth on relative grain size as observed by Sheppard et al. (1995, 1999). This positive trend may be 348 349 due to increased turbulence caused by larger bed roughness elements or the initiation of larger-scale scour 350 processes around coarser particles under certain flow conditions (Whitehouse, 2010). 351 Furthermore, a significant positive correlation was found with the Keulegan-Carpenter number with a correlation 352 factor of 0.81, indicating the importance of oscillatory flow conditions in scour development. Higher Keulegan 353 Carpenter number directly leads to higher relative scour depth (Sumer and Fredsoe, 2002). This is driven by the 354 onset of the horseshoe vortex and lee-wake eddy shedding (Sumer et al., 1992b; Zanke et al., 2011), with increased 355 permanence of the horseshoe vortex and amplification of bed shear stresses at higher KC values (Sumer et al., 356 1997). In addition, the mobility parameter exhibits a strong positive correlation (0.71) with the relative scour depth. The mobility parameter quantifies the instantaneous capacity of the flow to exceed the entrainment threshold, 357 358 driving rapid sediment entrainment when significantly above unity (Soulsby, 1997; van Rijn, 1993). Variables 359 such as the pile Reynolds number, the flow intensity, and the Froude number, although less correlated with relative scour depth, contribute more to the total variance. This suggests that these flow-related variables influence relative 360 scour depth through more complex or non-linear interactions with other hydrodynamic conditions and sediment 361 362 characteristics. 363 Since seabed sediment characteristics play a significant role to local scour (Qi et al., 2016), the PCA was applied 364 again to the same dataset but pre-clustered into different soil classes (Annad et al. 2021). By reducing the 365 uncertainties related to grain size (d_{50}) , this analysis should provide a better estimation of the local scour. This classification also facilitates the identification of parameters that are more influential in estimating scour for 366 367 specific soil classes rather than uniformly across different types. After the clustering, six soil classes were obtained: 368 cohesive sediment ($d_{50} \le 63 \mu m$) with 5 data points, fine sand ($63 \le d_{50} < 200 \mu m$) with 203 data points, medium sand $(200 \le d_{50} < 630 \ \mu m)$ with 249 data points, coarse sand $(630 \le d_{50} < 2000 \ \mu m)$ with 170 data points, fine 369 gravel $(2000 \le d_{50} < 6300 \,\mu\text{m})$ with 18 data points, and medium gravel $(d_{50} \ge 6300 \,\mu\text{m})$ with 49 data points. 370

3.72 3.3 Principal component analysis (PCA) by clustered soil classes

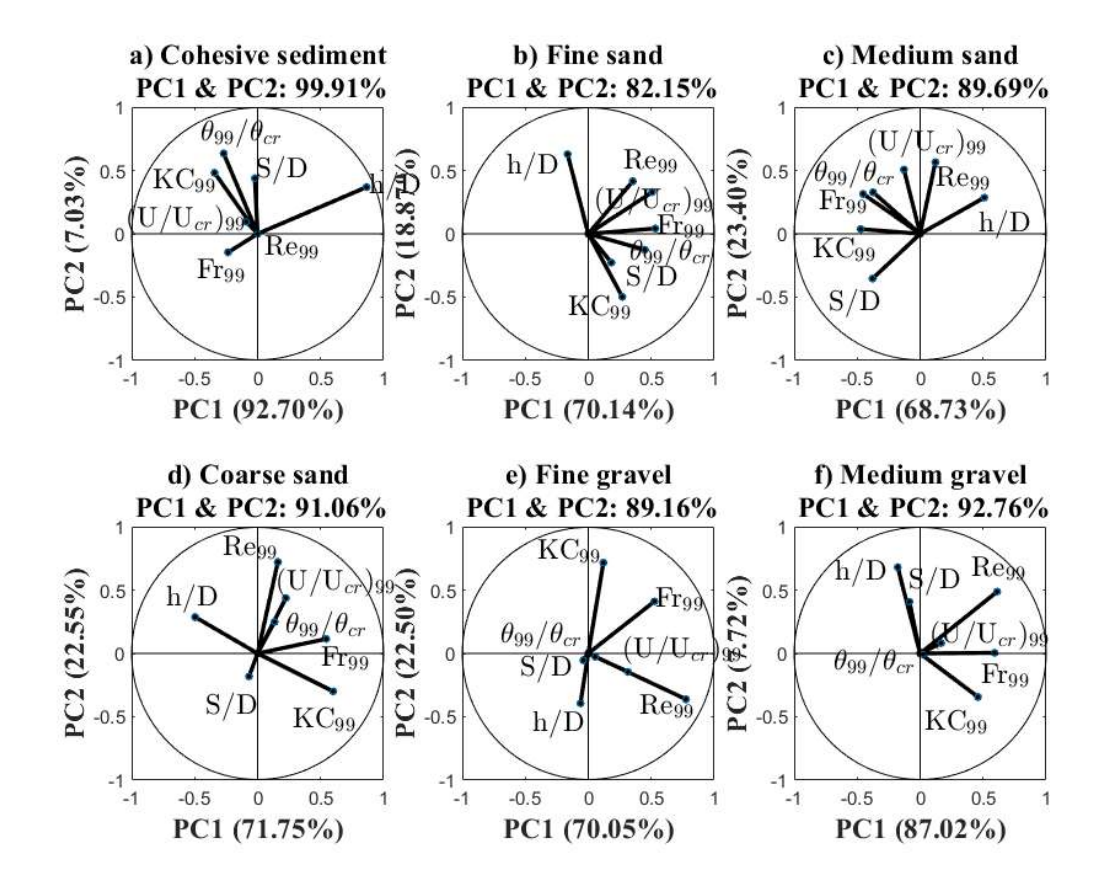


Figure 5: PCA correlation by clustered soil classes based in the grain size (d_{50}) , remaining parameters that are shown in the biplots are explain in data description (section 2.2). a) Cohesive sediment $(d_{50} \le 63 \ \mu m)$. b) Fine sand $(63 \le d_{50} < 200 \ \mu m)$. c) Medium sand $(200 \le d_{50} < 630 \ \mu m)$. d) Coarse sand $(630 \le d_{50} < 2000 \ \mu m)$. e) Fine gravel $(2000 \le d_{50} < 6300 \ \mu m)$. f) Medium gravel $(d_{50} \ge 6300 \ \mu m)$. Clustering of the grain size (d_{50}) was based on Annad et. al. (2021).

374

375

376

377

378

390

379 Building on the initial PCA analysis, which emphasized the significant influence of grain size on relative scour 380 depth, a more detailed investigation was conducted by categorizing the dataset into six soil classes: cohesive 381 sediment ($d_{50} \le 63 \ \mu m$) with 5 data points, fine sand ($63 \le d_{50} < 200 \ \mu m$) with 203 data points, medium sand $(200 \le d_{50} < 630 \,\mu m)$ with 249 data points, coarse sand $(630 \le d_{50} < 2000 \,\mu m)$ with 170 data points, fine gravel 382 383 $(2000 \le d_{50} < 6300 \ \mu m)$ with 18 data points, and medium gravel $(d_{50} \ge 6300 \ \mu m)$ with 49 data points. 384 Figure 5 shows PCA biplots for each soil class illustrating the relationships between relative scour depth the 385 relative water depth, the Keulegan-Carpenter number, the mobility parameter, the pile Reynolds number, the 386 flow intensity and the Froude number. The first two principal components (PC1 and PC2) explain between 82.15 387 % and 99.91% 388 of the variance within each class, thus describing more of the variance in comparison to when the PCA was applied 389 to all data. Data complexity seems to be greatly reduced by just removing the effect of sediment. In the cohesive

sediment soil class (Figure 5a), relative scour depth is positively correlated with the mobility parameter. However,

the calculation of the mobility parameter might contain larger uncertainties for cohesive soils (Soulsby, 1997), so the results should be treated with caution.

In contrast, relative water depth has a strong negative correlation with relative scour depth in fine sand (Figure 5b) 393 and medium sand (Figure 5c). This indicates that as relative water depth increases, relative scour depth tends to 394 395 decrease in these finer soil classes. From a physical view, Melling (2015) found out that in similar substrates, 396 relative scour depth agree well between different geographic locations and showed that OWES located in sandy 397 sediments exhibit a strong influence of relative water depth on scour, suggesting geotechnical factors are less 398 influential in coarser sediments. Although the observation that relative scour depth decreases as relative water 399 depth increases might initially seem counterintuitive. This behavior is best explained through the transition between shallow-water and deep-water flow regimes. As flow approaches a pile, stagnation pressure develops on 400 401 its upstream face, causing the flow to separate into an up-flow and a down-flow component. The down-flow is 402 directed toward the bed and promotes the formation of a horseshoe vortex. Flow separation occurs at the stagnation 403 point, defined as the location of maximum energy from the approaching flow at the pile face. The energy of the 404 approach flow consists of hydrostatic and kinetic components, whose vertical distribution is governed by the 405 boundary layer. In shallow water, the kinetic component dominates over hydrostatic pressure, resulting in a stagnation point located higher up the pile, near the water surface. This enhances down-flow and vortex activity, 406 intensifying scour processes (Melville, 2008). Additionally, shallower water often features thinner boundary layers 407 408 with higher velocity gradients near the seabed, potentially leading to greater bed shear stresses and increased 409 sediment mobility. In contrast, in deeper water, hydrostatic pressure becomes more influential, leading to a more 410 uniform pressure field across the pile face and shifting the stagnation point closer to the bed. This results in weaker 411 down-flow and reduced vortex strength, thereby diminishing the scour depth (FHWA, 2012; Harris & Whitehouse, 2014). Furthermore, Link and Zanke (2004) observed that maximum relative scour depth tends to develop more 412 413 slowly and reach lower values in deeper water depth, even under constant average flow velocity, due to reduced 414 shear velocity over the undisturbed bed. This highlights that the relationship between relative water depth and 415 scour is not necessarily linear.

The dynamics observed in coarse sand (Figure 5d) and fine gravel (Figure 5e) are different from the finer sediments. In these classes, the flow intensity and the Froude number show significant negative correlations with relative scour depth, indicating that higher values of these parameters correspond to reduced relative scour depth. However, these soil classes are also characterized by comparatively small relative scour depth, which makes the relationship less prominent.

For medium gravel (Figure 5f), relative water depth has a positive correlation with relative scour depth, meaning that greater relative water depth are associated with greater relative scour depth in coarser sediments. The data points in the cluster can be attributed to the Humber Gateway OWF, which is the only OWF that features clearwater conditions. Given the large grain sizes, a smaller influence of flow parameters on the variability of relative scour depth should be expected.

426

427 3.4 Correlation of scour depth with main drivers

Following the PCA (Figure 5), which identified the primary variables influencing relative scour depth across soil classes, a Pearson correlation analysis was performed to quantify the strength and direction of these relationships.

430 Figure 6 shows the Pearson correlation results for each cluster and the variable with the strongest correlation, with

the red lines representing the linear regression fit and the correlation coefficients shown in red text. The Pearson correlation was calculated by the following equation:

$$R = \frac{\sum (x_i - \bar{x})(y_i - \bar{y})}{\sqrt{\sum (x_i - \bar{x})^2 \sum (y_i - \bar{y})}} \dots (9)$$

Considering the small number of data points in this sediment cluster, relative scour depth at locations with cohesive sediments (Fig. 6a) show a moderate correlation between scour with the mobility parameter. For the fine and medium sand clusters, the PCA revealed a similarly strong dependence of relative scour depth on relative water depth. Plotting relative scour depth against relative water depth now shows a clearer trend and hence dependence for the medium sand sites (Fig. 6c) than for the fine sand sites (Fig. 6b). The Pearson coefficients of -0.57 and -0.86 confirm this difference in the dependence of relative scour depth on relative water depth. The correlations of the fine and medium sand clusters are supported by a larger number of data points, increasing the reliability of the findings.

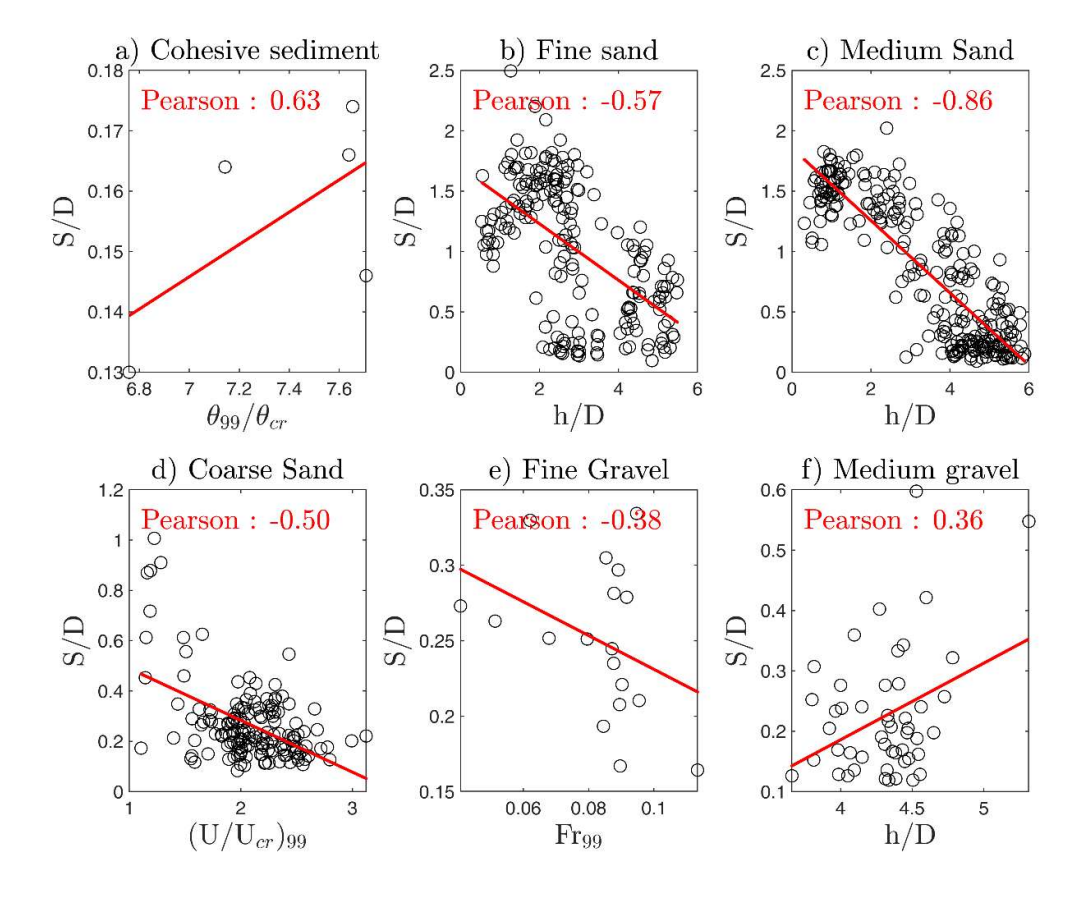


Figure 6: Pearson correlation of representative variables obtained by PCA analysis with relative scour depth across different soil classes. a) Cohesive sediment ($d_{50} \le 63 \,\mu m$). b) Fine sand ($63 \le d_{50} < 200 \,\mu m$). c) Medium sand ($200 \le d_{50} < 630 \,\mu m$). d) Coarse sand ($630 \le d_{50} < 2000 \,\mu m$). e) Fine gravel ($2000 \le d_{50} < 6300 \,\mu m$). f) Medium gravel ($d_{50} \ge 6300 \,\mu m$).

For the coarse sand (Figure 6d), the PCA analysis revealed a negative correlation between relative scour depth and flow intensity. This result directly aligns with the established understanding of live-bed scour behavior in coarse-

grained sediments. Once flow intensity surpasses the critical threshold ($(U/U_{cr})_{99}$ >1), the sediment mobilizes, 450 establishing live-bed conditions. In such scenarios, the development of large, well-defined scour holes is consistently observed to be suppressed. This suppression occurs because the continuous transport and 451 452 replenishment of sediment into the scour region actively works against deep erosion. This dynamic equilibrium of 453 the seabed results in shallower, or inherently more unstable, scour holes when compared to clear-water conditions. In clear-water, where sediment remains immobile, scouring is driven purely by flow-induced vortex action around 454 455 the structure (Sumer & Fredsøe, 2002; Whitehouse et al., 2011). Consequently, the negative correlation observed 456 in this soil class accurately reflects the inherent limitation of scour growth under the highly mobile conditions 457 characteristic of coarse sandy beds. 458 For fine gravel (Figure 6e), the PCA suggests a correlation between relative scour depth and the Froude number, 459 but this is difficult to confirm visually due to the small sample size and narrow Froude number range. Since relative 460 scour depth is comparatively small in this class, relationships are less clear, and parameters like Froude 461 number come to the foreground that were not as prominent in finer sediments. A broader distribution of Froude 462 number values would be necessary to confirm this more conclusively. 463 Finally, medium gravel (Figure 6f) displays a positive correlation between relative scour depth and relative water 464 depth, with a Pearson coefficient of 0.36. This indicates that larger relative water depth correspond to increased 465 scour depth, although the range of this increment remains small (between S/D = 0.1 and S/= 0.4). This variation 466 in scour depth is small compared to the correlations observed in fine and medium sands, where changes in relative water depth yield more pronounced differences in relative scour depth. The smaller impact in medium gravel may 467 468 be attributed to the generally greater resistance of larger sediments to scour, even with increasing relative water 469 depth. 470 The most significant correlations emerge from the fine sand (Figure 6b) and medium sand (Figure 6c), where strong negative correlations between relative scour depth and relative water depth are observed. This suggests that significant scour occurs in shallower waters with finer sediments. Such findings highlight the importance of 472 473 relative water depth as a key factor influencing scour processes in specific sediment types, emphasizing that scour 474 management and predictions for offshore structures should take sediment characteristics and relative water depth 475 into account. These results are consistent with the studies from Melling (2015) and Harris and Whitehouse (2014), 476 which also show a decrease in relative scour depth in finer sediments as relative water depth increase. This negative 477 correlation can be explained by the reduction in bed shear stress with increasing relative water depth, which limits 478 sediment mobilization, particularly in fine and medium sands (Sumer & Fredsøe, 2002; Fredsøe & Sumer, 2014). 479 However, those results disagree with experimental work where scour around a monopile weakens with reducing relative water depth (e.g. May and Willoughby, 1990; Whitehouse, 1998). Consequently, relative water depth is 480 481 included as a parameter in many empirical formulas, especially in for scour around bridge piles with limited water 482 depth (eg., Laursen, 1963; Hancu, 1971; Breusers et al., 1977; May and Willoughby, 1990; Richardson et al., 483 2001). Besides that, these insights from field data are critical for the accurate assessment and planning of offshore infrastructure installations, particularly in regions with varying sediment characteristics.

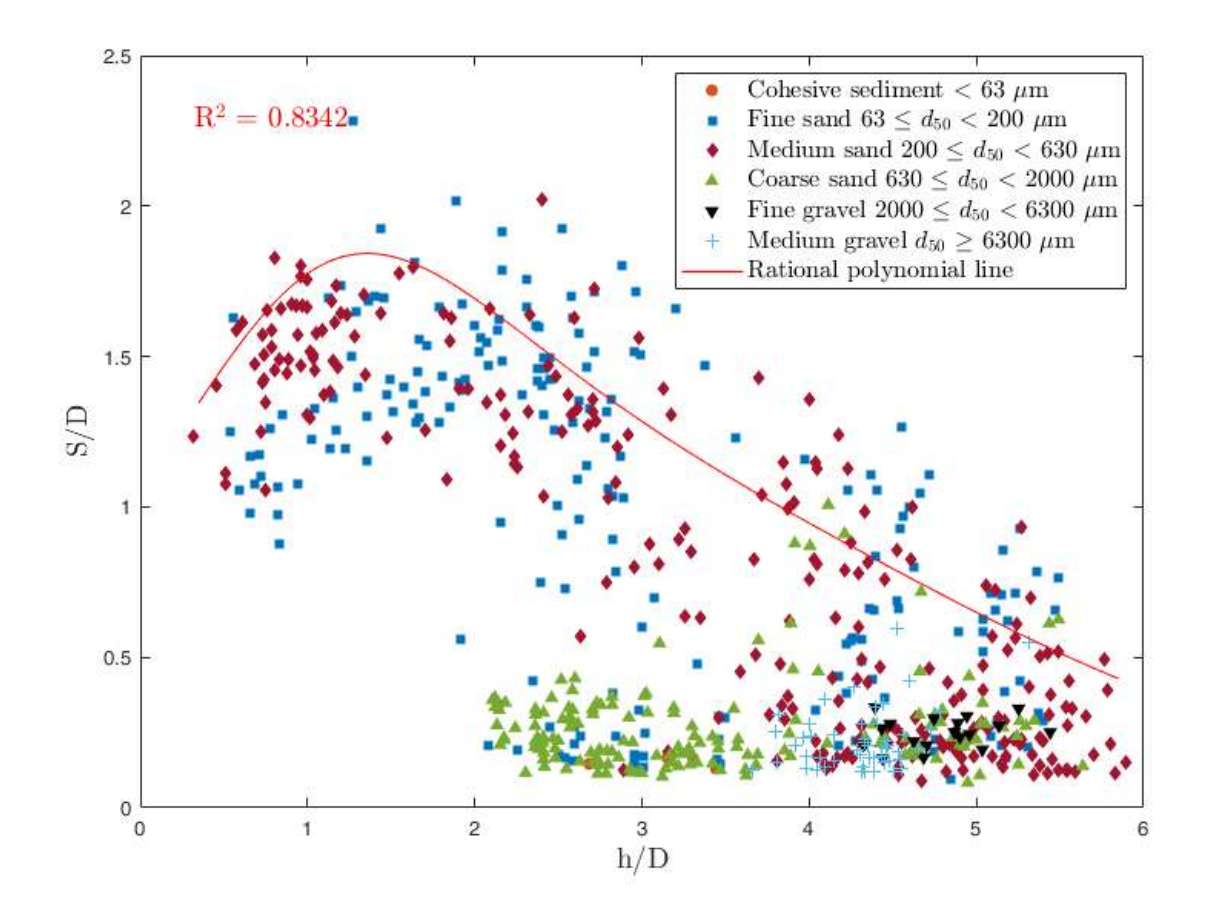


Figure 7: Relative scour depth vs relative water depth, and soil classes. The red rational polynomial line represents a trend based on the course of the 99th percentile. Data points for London Array and Thanet OWFs are included from Melling (2015).

Figure 7 summarizes the findings from the PCA analysis (Figure 4) by plotting the relationship between the relative scour depth and the relative water depth. Relative water depth has shown to be the parameter with the largest correlation influencing relative scour depth. However, it should be noted that relative water depth has a direct effect on other hydrodynamic parameters. For example, not only is the Froude number formed with the water depth, but relative water depth also significantly determines the potential influence of waves on the development of scour, which in this study has also been considered by the Keulegan–Carpenter number. Therefore, it remains unclear whether the influence of relative water depth on relative scour depth is a direct causal factor or an indicator of broader changes in hydrodynamic conditions. Nevertheless, Figure 7 illustrates the comprehensive correlation between the relative scour depth and the relative water depth with the differently colored points representing the studied soils classes.

The trend observed in Figures 6b and 6c is reaffirmed in Figure 7. A distinct relationship exists between the relative scour depth and relative water depth in these two sediment types, i.e. both fine sand ($63 \le d_{50} < 200 \ \mu m$) and medium sand ($200 \le d_{50} < 630 \ \mu m$) show that the relative scour depth decreases with increasing relative water depth. This trend appearing throughout the bigger dataset emphasizes a strong negative correlation between relative water depth and relative scour depth for those soil classes. This behavior is consistent with findings from

previous analyses that identified relative water depth as a critical factor in shaping scour dynamics (Whitehouse et al., 2010 and Melling, 2015).

In contrast, for sediments with median grain diameters above coarse sands ($d_{50} \ge 630 \, \mu m$) the relative scour depth remains relatively constant and shows little variability. Figure 7 suggests a generally stable relationship between relative scour depth and relative water depth for these soil classes, where changes in relative water depth do not significantly alter relative scour depth. However, there are a few exceptions. For example, some locations with coarse sand located in deeper water exhibit unexpectedly large relative scour depth. These outliers might stem from site-specific conditions such as dynamic sandbanks and highly variable bathymetry, as seen at the London Array OWF (Sturt et al., 2009). These unique environments, characterized by flow recirculation and sediment mobility, can lead to deviations from expected scour behavior (Melling, 2015). The results for fine and medium sands suggest a potential influence of relative water depth in reducing relative scour depth. Although these results are preliminary, they provide a first step in understanding how offshore wind OWES could affect sediment redistribution in regions dominated by these sediment types and small relative water depth.

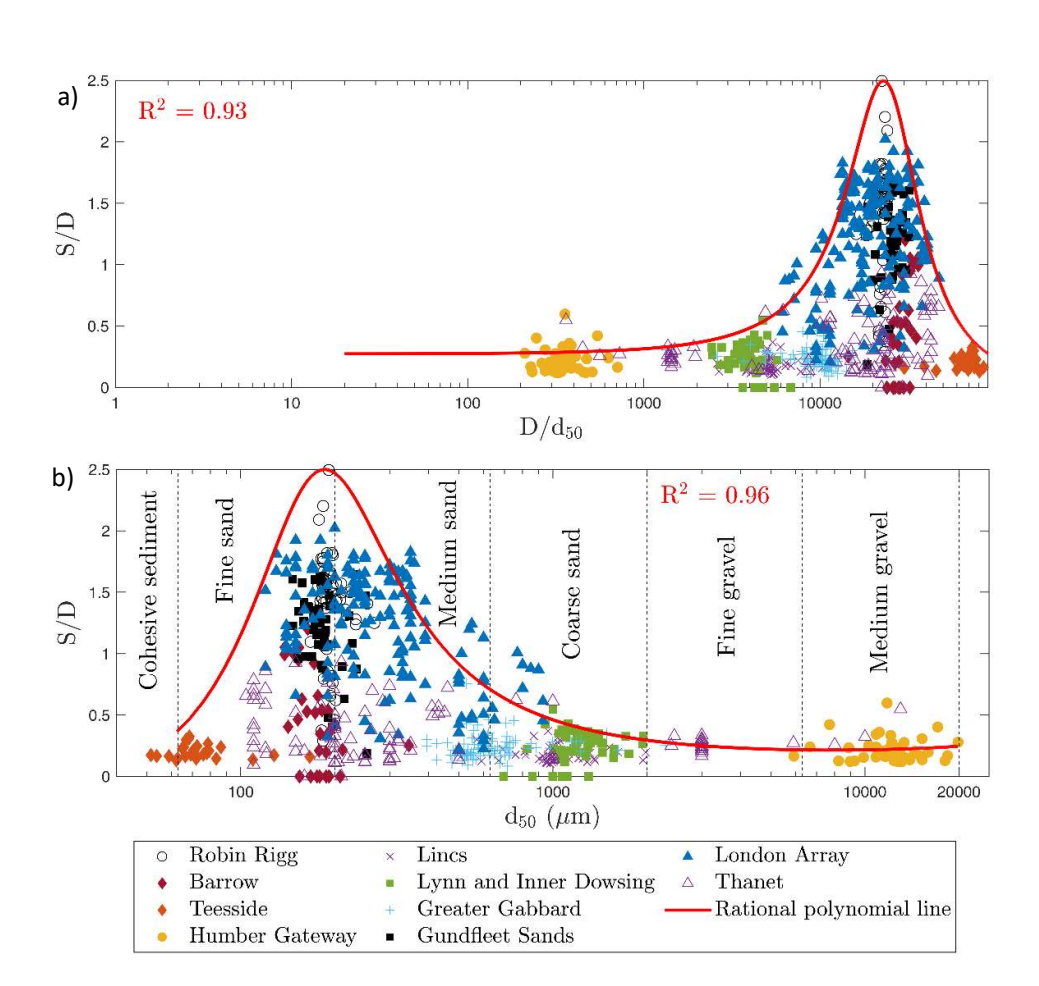


Figure 8: Relative scour depth against (a) the relative grain size, and (b) grain size. The red rational polynomial line gives the approximate upper limit of S/D, based on the course of the 99th percentile, for various d_{50} . Data points for London Array and Thanet OWFs are included from Melling (2015).

Figure 8a summarizes the findings from the PCA analysis (Figure 4) by plotting the relationship between the relative scour depth and relative grain size across all the sampled locations. Figure 8b is also shown here to support

figure 8a by representing the data in terms of the grain size, allowing the comparison of dimensional and non-524 525 dimensional relative grain size. Figure 8a, reveals no clear trend between relative scour depth and relative grain size, indicating that the dimensionless grain size ratio alone does not adequately capture the relationship between 526 sediment properties and scour depth in field data. Sheppard et al. (2004) observed a clear trend of S/D decreasing 527 for $^D/_{d_{50}} > 50$ in laboratory experiments, which is not consistent with our results. However, field data show 528 529 much weaker dependence due to natural variability in sediment structure and hydrodynamic forcing 530 On the other hand, Figure 8b illustrates a discernible trend where the largest relative scour depth occurs predominantly in fine to medium sands (R2= 0.8407), as indicated by the rational polynomial line which 531 approximates the upper limit of relative scour depth for various grain size. The trend shown in Fig. 8b is well 532 533 explained. In general, the mobility potential of the sediments decreases with increasing grain size, which leads to 534 lower relative scour depth for coarser sediments. Very fine sediments, on the other hand, are subject to the 535 influence of cohesion forces that reduce their erodibility, which also leads to lower relative scour depth. Therefore, 536 fine and medium sandy sediments have the largest scour potential, which is reflected in the data of Fig. 8b. The different symbols represent the OWF, highlighting the geographic spread and variability within the dataset. 537 However, it is important to note that most of the data points fall within the range of fine to medium sands, 538 539 potentially skewing the interpretation.

540

541

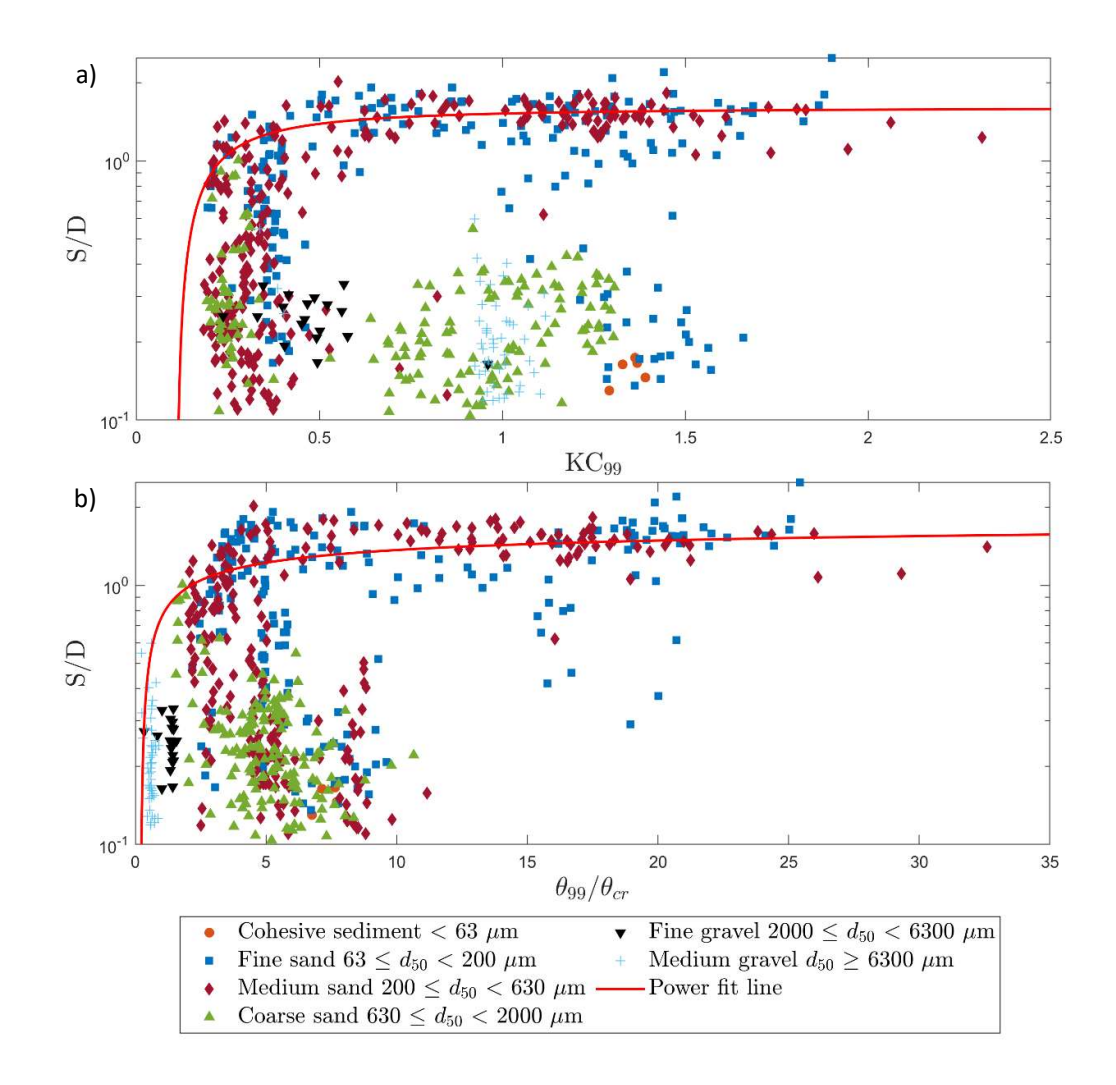


Figure 9: Relative scour depth against the a) Keulegan-Carpenter number and b) the mobility parameter. Red line gives the power fit line based on the 99th percentile of the data of relative scour depth for various d_{50} . Data points for London Array and Thanet OWFs are included from Melling (2015).

The third and fourth parameters, that correlate with the relative scour depth, are the Keulegan-Carpenter number and the mobility parameter as identified by the PCA. Figure 9a shows the correlation between the relative scour depth and the Keulegan-Carpenter number, revealing a distinct increase of relative scour depth with increasing Keulegan-Carpenter number up to $KC_{99} = 0.5$. Above this value, relative scour depth shows little variation with further increase of the Keulegan-Carpenter number, which reaches a maximum value of 2.5 in this field dataset. Those results are generally consistent with findings from previous studies (e.g., Qu et al., 2024; Sumer & Fredsøe, 2002), which indicate that scour development is strongly dependent on KC_{99} at lower values, but becomes less sensitive as KC_{99} increases. However, experimental studies often focus on wave regimes with KC numbers greater than 6, since it has been established that this is the threshold for generating a horseshoe vortex. Despite considering the 99th percentile of KC numbers over the time period in question, the KC numbers are much smaller for the field conditions presented herein. This strengthens the argument for further scour research to focus on boundary conditions with low KC values.

Figure 9b shows the correlation between relative scour depth and mobility parameter, comparing the Shields 559 560 parameter with its critical threshold for sediment motion, and revealing a distinct increase of relative scour depth with increasing mobility parameter up to approximately $\theta_{99}/\theta_{cr}=5$. At higher mobility values (typically above 5– 561 562 10), the increase in scour depth tends to stabilize. This trend aligns with experimental observations from Sumer et 563 al. (2013), Chiew (1984), and others, which describe similar stabilization of scour depth under fully mobile 564 conditions. Notably, the response also varies with sediment type: coarser sediments exhibit low relative scour 565 depth values even at high mobility ratios, likely due to their higher resistance to entrainment and potential armoring effects. In contrast, finer sediments (e.g., $d_{50} < 200 \ \mu m$) show a steeper increase in scour depth, reflecting their 566 567 greater susceptibility to hydrodynamic conditions.

Overall, Figure 9a and 9b emphasize the nonlinear and sediment-dependent nature of scour formation. The separation of trends by soil class supports the need for sediment-specific scour prediction models, as also suggested in previous studies (e.g., Whitehouse et al., 2011; Sumer & Fredsøe, 2002). The results provide empirical evidence of this dependency using field-scale data, bridging a critical gap between controlled experiments and real-world conditions.

573

574 3.5 Detailed analysis of scour patterns for selected OWFs

Following the observed overall trend shown in Figure 7, this section moves on to examine scour patterns within individual OWFs, such as Robin Rigg, Lynn and Inner Dowsing, and London Array. This specific analysis will assess whether the global relationship between relative scour depth d_{50} , and relative water depth holds under the unique environmental conditions of each site. This section aims to further our understanding of the dynamics between sediment characteristics and scour processes by a detailed analysis of the variation within each wind farm to determine if these global correlations are consistent at the local scale or if there are deviations due to site-specific factors.

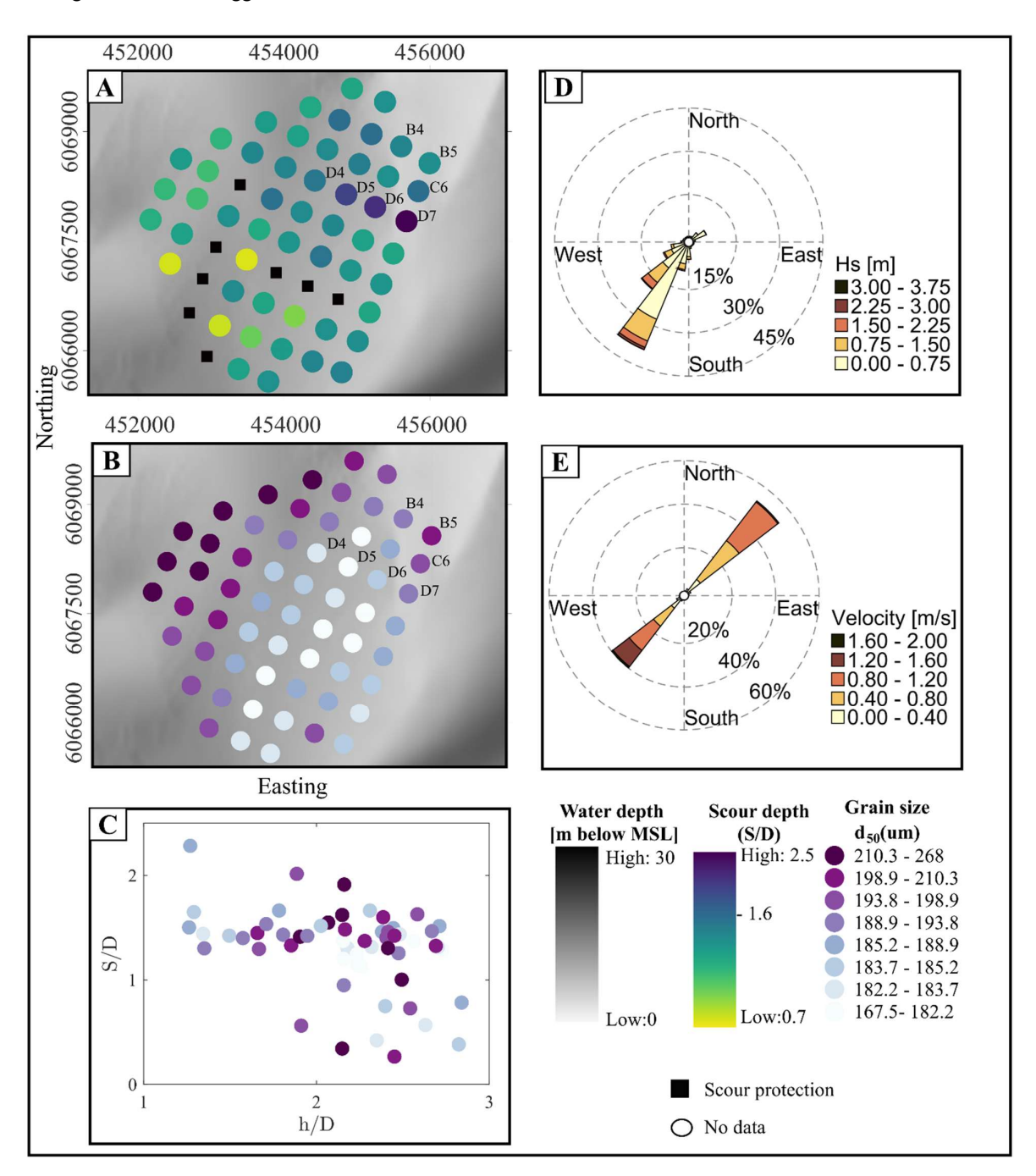
3.5.1 Robin Rigg OWF
Robin Rigg is presented and discussed in this section as this OWF has the largest overall relative scour depth of
all the OWFs. This detailed analysis will help to investigate whether the negative correlation between relative
scour depth and relative water depth observed globally in Figure 7 holds true under variable geotechnical
conditions, taking into account that sediment grain sizes range from fine to medium sands.
Figure 10 shows the distribution of relative scour depth at Robin Rigg in relation to the variable geotechnical and

hydrodynamic site conditions. This sequence begins with Figure 9A, showing the spatial distribution of scours measured one year after turbine installation. A significant variation in relative scour depth in different areas of the OWF can be observed, with the deeper relative scour depth mainly located in the northeastern part, particularly around OWES D7, C6, B5 and B4, which are located in the shallowest waters. Figure 10B shows the spatial distribution of the median grain diameter d_{50} in the uppermost sediment layer in 2005, with sediment sizes predominantly in the range of fine to middle sand (182 μ m to 268 μ m). OWES in areas with finer sands, such as D4, D5, and D6, are observed to generally experience the large scour, consistent with previous observations by

Whitehouse (2006) that finer sand substrates are more susceptible to scour.

Figure 10C shows the correlation of relative scour depth and relative water depth, classified by colored points which represent sediment grain size from figure 9B. Contrary to the clear negative correlation between relative scour depth and relative water depth observed globally in Figure 8, Figure 10C shows a wide distribution of data points with no clear trend, suggesting that local factors in addition to relative water depth and sediment type have an influence on scour at this site.

For additional insight, Figures 10D and 10E show the distribution of the directions of significant wave heights, as well as the directions of current velocity magnitudes one-year period, prior the post scan. The highest wave heights came predominantly from the southwest, which should influence sediment mobility and thus scour structures along this direction and especially in shallow relative water depth where wave-induced shear stresses should be higher. Similarly, the tidal current, with its main directions of south-west and north-east, should result in a change in relative scour depth along this main axis. However, a clear trend of relative scour depth changing in this direction is not given for Robin Rigg.



- 609 Figure 10: A) Spatial distribution of relative scour depth from 2008-2009 at Robin Rigg OWF. B) Grain-
- 610 size distribution. C) Relative scour depth vs relative water depth, and grain size classification D) Significant
- 611 wave heights E) Current velocities.
- 612 This comprehensive analysis using Figures 10A to 10E shows that while correlations obtained from global findings
- 613 provide a useful baseline for understanding scour, the actual scour observed at Robin Rigg does not necessarily
- 614 follow those correlations. While the distribution of relative scour depth appears to be strongly influenced by local
- 615 environmental conditions such as sediment type, waves and currents, the dominant influence among these cannot
- 616 be clearly identified, rather the distribution of relative scour depth appears to be due to the interaction of all
- 617 influences.
- 618 The discrepancies between the local scour behavior at Robin Rigg and the broader correlations observed in Figure
- 619 8 underscore the need for site-specific assessments. Such detailed analyses are critical to the development of
- 620 effective scour management and mitigation strategies tailored to the unique conditions of each offshore wind farm.

621 3.5.2 Lynn and Inner Dowsing OWF

- 622 Lynn and Inner Dowsing was chosen as a further example as this OWF had the lowest relative scour depth of all
- 623 the OWFs investigated and is also characterized by coarse to very coarse sands. Figure 11 provides the same
- 624 analysis as Figure 10 by providing insight into how local conditions compare to the global trend seen in Figure 7.
- Figure 10A shows the spatial distribution of relative scour depth measured from 2007 to 2010. Figure 11A shows
- 626 that the largest relative scour depth are mainly concentrated in the Inner Dowsing area, especially around OWES
- 627 ID1, ID2, ID8, ID9, ID12, ID24, and ID30. Except for turbine L21, which has the deepest relative scour depth in
- 628 the entire wind farm and which is located at the southeastern end. The significant relative scour depth observed at
- 629 certain locations (e.g., D30, L21) are related to cable exposure (EGS Ltd, 2012; EGS Ltd, 2013), while smaller
- 630 relative scour depth are more common in the southern region. Overall, the spatial distribution shows a slight trend
- 631 of increasing relative scour depth from south to north.

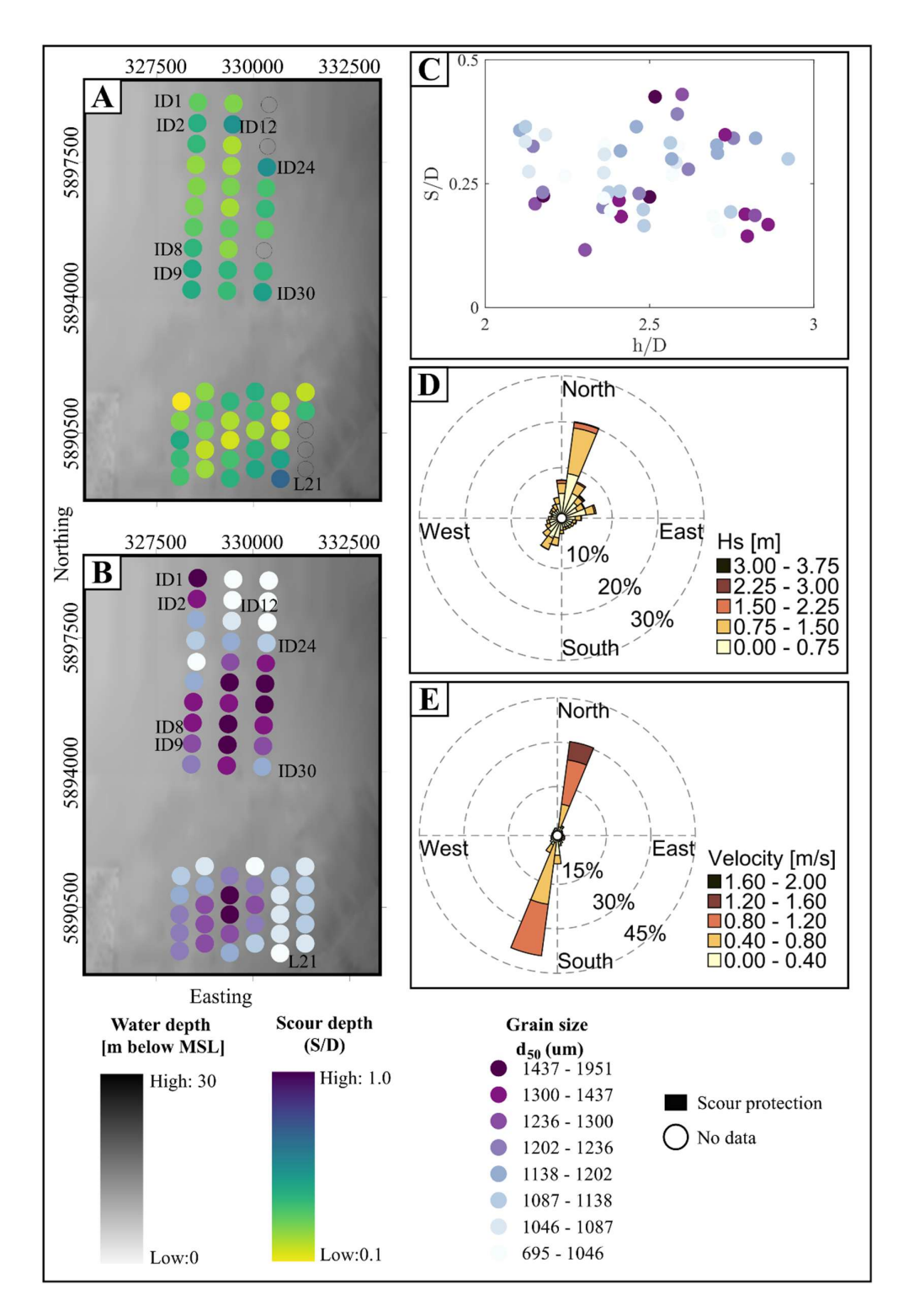


Figure 11: A) Spatial distribution of relative scour depth at Lynn and Inner Dowsing OWF from 2007-2010.
 B) Grain-size distribution. C) Relative scour depth vs relative water depth, and grain size classification. D)
 Significant wave heights E) Current velocities.
 Continuing with the spatial overview, Figure 11B introduces the spatial distribution of d₅₀ median grain sizes,
 which shows a range from coarse to very coarse sands (695 to 1951 μm). The correlation between relative scour

- 639 negative correlation as seen globally in Figure 8, suggesting that additional local factors may significantly
- 640 influence relative scour depth.
- 641 Consequently, the significant wave heights and current velocities from hindcast data are shown in Figure 10D and
- 642 10E. The highest wave heights, observed from the northeast, and strong tidal currents flowing from southwest to
- 643 northeast, highlight the dynamic environmental forces at play. The presence of the largest relative scour depth in
- 644 the Inner Dowsing area align with the direction of the highest tidal current velocities (Fig. 11E) recorded in the
- 645 northeast part as well the main direction of waves. Therefore, the direction of both tidal current and waves likely
- 646 play a significant role for the scour development in this wind farms, as the seabed conditions and relative water
- 647 depth locally do not exhibit a distinct correlation.

648 3.5.3 London Array OWF

- 649 Following the previous results, the analysis for London Array OWF shows a wide range of relative scour depth
- from S/D = 0.2 to S/D = 2.1. This variability differs markedly from the consistently larger relative scour depth
- 651 observed at Robin Rigg and the limited maximum depth of up to S/D = 1.0 at Lynn and Inner Dowsing. "The
- area of London Array OWF is characterized by an alternating pattern of deep channels (Black Deep, Knock Deep)
- and sandbanks (Long Sands, Kentish Knock). These topographic features significantly contribute to the local scour
- 654 patterns. Water depth at this site range from 0 to 30 m, with Long Sands known for its significant variations in bed
- 655 elevation but general stability of position. Meanwhile, Knock Deep is notable for its eastward shift over time,
- which has widened the channel and maintained a constant bed level.

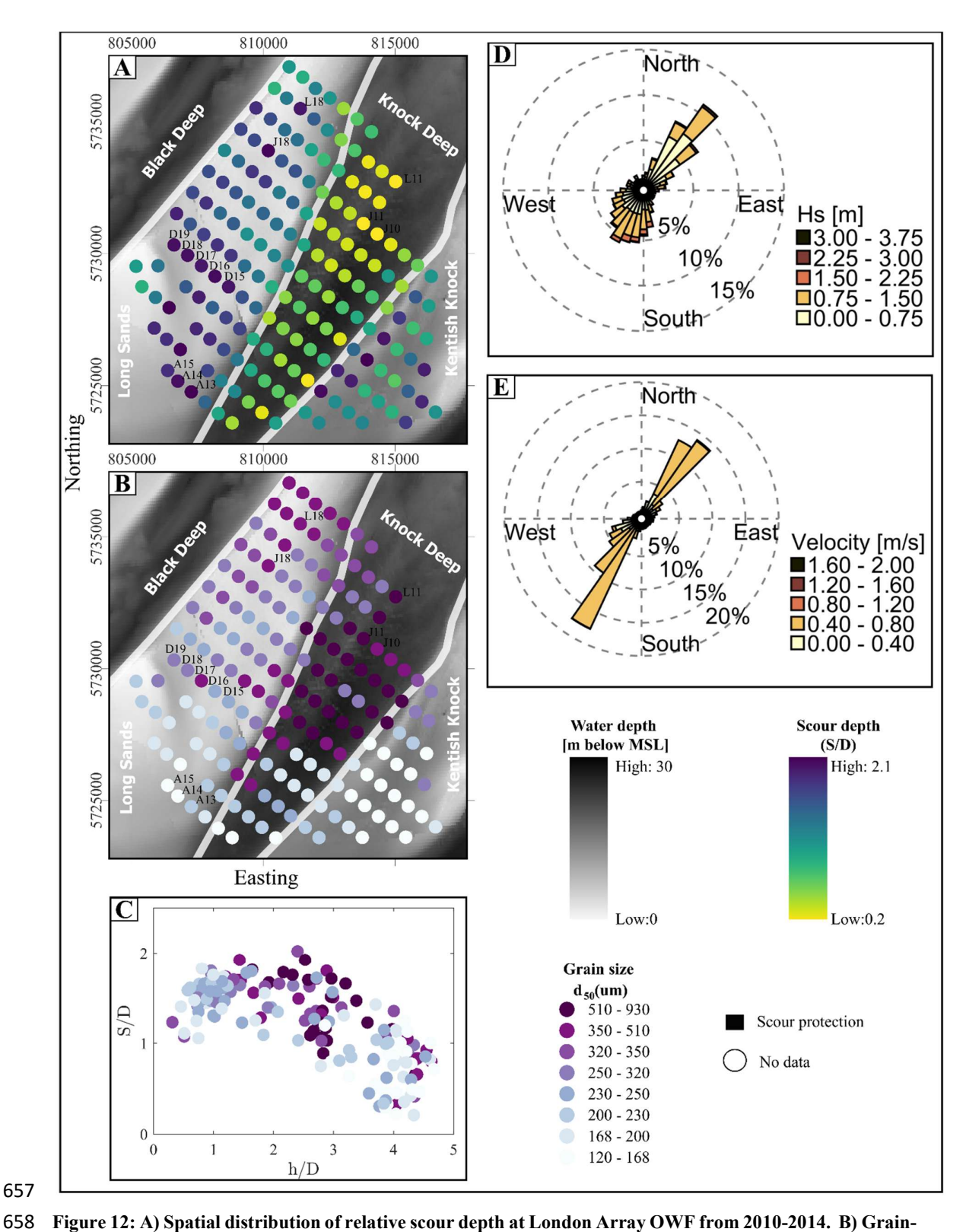


Figure 12: A) Spatial distribution of relative scour depth at London Array OWF from 2010-2014. B) Grainsize distribution. C) Relative scour depth vs relative water depth, and Grain size classification. D) Significant wave heights and E) Current velocities. Relative scour depth and grain size data are used from Melling (2015)

660

In Figure 12A, the distribution of relative scour depth shows that the variation in scour is strongly influenced by 663 the underlying topography, with significantly greater relative scour depth on the sand banks compared to the channel. Additionally a trend of increasing relative scour depth is observed from northeast to southwest, which is 664 particularly notable in the channel area. The smallest scour is observed in the northern part of Knock Deep with a 665 666 ratio of S/D = 0.2 and the largest in the southern part of Long Sands with S/D = 2.1. The differences in relative 667 scour depth can be derived directly from the seabed topography, with greatest average relative scour depth found in the Long Sands with S/D = 1.53, followed by Kentish Knock (S/D = 1.37), and then Knock Deep (S/D = 1.37). 668 669 0.77) with the smallest average. The sediment distribution across this OWF, shown in Figures 12B, ranges from very fine to coarse sands. Coarse sands can be found in Knock Deep, where generally the smallest relative scour 670 671 depth are seen (e.g., L11, J10 and J11). Furthermore, the largest relative scour depth are noticed in the southern 672 part of Long Sands (e.g. A13-A15, D15-D19, J18 and L18), where the sediment varies from very fine to fine medium sands. There is therefore a reasonable correlation between grain size and relative scour depth, which is 673 consistent with the previously observed global trend. Additionally, Figures 12C shows a negative correlation 674 675 between relative scour depth and relative water depth aligning with the global trend observed in Figure 8, i.e. that 676 shallower relative water depth can be associated with deeper scour, while deeper waters tend to have reduced relative scour depth. This trend may be explained by the findings of Hjort (1975), who demonstrated that bed shear 677 678 stress decreases with increasing relative water depth for the same flow and structure diameter, potentially leading 679 to reduced scour at greater depth. However, as the relative water depth in the London Array OWF changes simultaneously with the sediments, i.e. coarser grained sediments are present in the deeper water depth of Knock 680 681 Deep, the cause of the different relative scour depth cannot be clearly attributed to either the sediments or the water 682 depth. Other hydrodynamic, environmental, and topographic factors also play a critical role in shaping these 683 patterns at this OWF, underscoring the complexity of the influences involved. Significant wave heights and current velocities, as shown in figures 12D and 12E, provide important insights into 684 685 the scour dynamics at the London Array. These figures show that, in addition to relative water depth and sediment grain sizes, wave and current dynamics might be critical factors at this wind farm. The predominant direction of 686 687 both waves and currents is northeast to southwest, consistent with the estuarine influence of the area, where river 688 discharge also significantly affects hydrodynamic conditions. This influence is particularly evident at the Long 689 Sands and Kentish Knock sandbanks, which are shaped by the combined action of waves and currents (London 690 Array Ltd, 2005). 691 Figures 12D shows that the highest wave heights are observed coming from the northeast, with values exceeding 692 3.0 m, and lower wave heights propagating from the southwest. This gradient in wave height suggests a correlation 693 with increased relative scour depth in regions exposed to higher wave energy, suggesting a strong link between 694 wave dynamics and seabed modification. However, estimated KC99 numbers remained relatively low across most 695 sites, indicating limited wave-induced orbital motion near the seabed. This suggests that wave action plays a 696 secondary role in scour development compared to currents. Similarly, Figure 12E highlights a larger number of strong currents coming from the southeast. These higher velocities correspond to areas with more pronounced 697 698 relative scour depth, highlighting the role of strong currents in influencing sediment transport and depositional 699 patterns. 700 In addition, the local tidal dynamics vary significantly across the wind farm, with the flood tide dominating the 701 southern banks and the ebb tide more influential on the northern banks (Kenyon and Cooper, 2005). This variation

- 703 is particularly pronounced at Long Sands (London Array Ltd, 2005). The interplay of river discharge, wind stress,
- 704 tidal surge and density driven currents follow the pathways created by the existing topography, further
- 705 complicating the hydrodynamic environment and its effect on scour at the London Array OWF.
- 706 After analyzing the relative scour depth at 9 wind farms and with different ranges of relative scour depth, the
- 707 variation of relative scour depth can also be noticed in individual OWFs, as in the case for London Array OWF.

708 4. Discussion

709 4.1 Discussion of implications for scour predictions for OWFs

- 710 Overall, this study extends the investigation of scour dynamics to a regional scale by analyzing correlations
- 711 between relative scour depth and site conditions across multiple OWFs to identify consistent scour patterns and
- 712 correlations. The PCA analysis highlights a significant negative correlation between relative scour depth with
- 713 relative water depth, suggesting that relative water depth plays a critical role in scour processes, confirming the
- 714 correlations observed with previous Whitehouse et al. (2010) and Melling (2015) for field data. The decrease of
- 715 the relative scour depth with decreasing relative water depth seems unexpected and contradicts common scour
- 716 prediction approaches such as. Breusers et al. (1977), which however are often derived for flow conditions with
- 717 shallow relative water depth. Harris and Whitehouse (2014) argued that in deeper water, a weaker downflow and
- 718 hence a weaker horseshoe vortex can be expected, ultimately leading to smaller scour depth. This finding implies
- 719 that scour prediction approaches should place greater emphasis on relative water depth, particularly in offshore
- 720 environments where deeper flow conditions dominate.
- 721 A second notable correlation was identified between the relative scour depth with the relative grain size. This
- 722 broad correlation, consistent across different geographic locations and environmental conditions, reinforces the
- 723 fundamental role of sediment size in scour processes, as documented in the extensive work of Vanhellemont et al.
- 724 (2014) and Rivier et al. (2016).
- 725 However, the analysis also indicates that the sediment erodibility alone cannot fully account for the observed
- 726 variability in relative scour depth. The PCA analysis further reveals a positive correlation between the relative
- 727 scour depth and both the Keulegan Carpenter number and the sediment mobility parameter. The strong positive
- 728 correlation with KC₉₉ supports previous studies (Sumer and Fredsoe, 2001; Qu, 2024), highlighting the importance
- 729 of flow unsteadiness that is typical in tidal and wave-dominated environments. Similarly, the positive association
- 730 with the mobility parameter underscores its relevance as a key indicator of sediment entrainment and a useful
- 731 metric for distinguishing between different sediment transport regimes.
- 732 These findings underscore a complex dynamic that is frequently oversimplified in existing models. The results
- 733 indicate a necessity to incorporate nonlinear hydrodynamic models into scour prediction frameworks. The results
- 734 of the PCA reveal the necessity for a diversified approach to the modeling of scour in complex field conditions,
- 735 which extends beyond the scope of traditional uniform applications.
- 736 This analysis demonstrates that individual OWFs exhibit unique environmental and sediment conditions, which
- 737 can either amplify or moderate broader correlations. The London Array OWFs serves as a prime example of the
- 738 predictive reliability of observed regional correlations, as local data closely mirrors general correlations.
- 739 Conversely, sites such as Robin Rigg and Lynn and Inner Dowsing exhibit deviations from these correlations due
- 740 to their distinct sediment compositions and hydrodynamic conditions, underscoring the necessity for site-specific
- 741 adjustments to scour prediction models. These findings underscore the intricacy of employing global models on a

- 742 local scale and underscore the significance of site-specific data in validating and refining these models to enhance
- 743 their accuracy and applicability.

444 4.2 Discussion of limitations and future research

- 745 Although this study provides a detailed analysis of relative scour depth at nine OWFs, certain limitations must be
- 746 addressed to improve the interpretation of the findings. Although the dataset spans multiple years, it represents
- 747 snapshots in time and may not fully capture the dynamic evolution of scour processes under fluctuating metocean
- 748 conditions (Matutano et al., 2013; Carpenter et al., 2016). Hindcast data, while valuable for long-term correlations,
- 749 are often based on limited spatial resolution that may underestimate short-term extreme events such as storm surges
- 750 or localized current variations (Whitehouse et al., 2010; Sturt et al., 2009).
- 751 Using PCA is effective in identifying dominant linear relationships between relative scour depth and key variables;
- 752 however, it may miss critical nonlinear interactions that drive scour processes (Schendel et al., 2020; Lyu et al.,
- 753 2021). While this study incorporates, parameters such as the Keulegan-Carpenter number and the mobility
- 754 parameter, the accuracy of these parameters are limited by temporal resolution and data availability. Valuable
- 755 insight was provided into the role of hydrodynamic forcing on sediment mobility through their inclusion; however,
- 756 more detailed and site-specific input data are needed so that their predictive potential can be fully exploited
- 757 (Sheppard et al., 2004; Zhao et al., 2012).
- 758 The next step in this research is to develop data-driven models and investigate the broader implications for regional
- 759 sediment dynamics. Future studies will focus on OWFs located in fine and medium sands where significant scour
- 760 activity is observed. By focusing on these environments, we aim to improve prediction capabilities and better
- 761 understand the mechanisms that drive scour, particularly in areas that are susceptible to substantial sediment
- 762 mobilization.
- 763 Finally, while the present study focused on localized scour processes, the cumulative effects of OWF structures
- 764 on regional sediment transport and marine ecosystems remain a significant knowledge gap (Christiansen et al.,
- 765 2022; Schultze et al., 2021). Future research must employ interdisciplinary methodologies to rigorously assess the
- 766 ecological impacts of sediment mobility and scour on marine habitats. By integrating regional sediment transport
- 767 models with comprehensive ecological assessments, we can optimize offshore wind energy development to meet
- 768 both sustainability and environmental protection goals, ensuring long-term benefits for infrastructure resilience
- 769 and marine ecosystem health.

770 5 Conclusion

- 771 Achieving the European Union's (EU) offshore wind energy targets requires development of OWFs in regions
- 772 with diverse and often poorly understood meteoceanic and geophysical conditions. However, this demand
- 773 underscores critical knowledge gaps regarding the interaction of these installations with the marine environment,
- 774 particularly with respect to scour processes and sediment mobilization. A comprehensive understanding of scour
- 775 dynamics is essential, not only to ensure structural integrity, but also to assess potential impacts on regional
- 776 sediment transport and broader ecosystem functions.
- 777 In this study, high-resolution bathymetry data were used to analyze field-measured relative scour depth of 460
- 778 monopiles across nine British OWFs. The analysis included a PCA in which eight hydrodynamic and geotechnical
- 779 variables were considered to identify the dominant driver influencing relative scour depth variability. This analysis
- 780 provided a basis for understanding the primary correlations between relative scour depth and metocean site
- 781 conditions, but also highlighted the complexity of these relationships, requiring further refinement.

785

786

787

788

789

790

791

792 793

794

795

796

797

798

799

800

801

802

803

804

805

806

807

808

809

810

811 812

813

814

815 816

817

818 819

820

- (1) Universal drivers of scour: Across all nine OWFs, the PCA the relative water depth, the relative grain size, the Keulegan-Carpenter number and the mobility parameter as the most influential variables governing scour depth variability. Among these, the relative water showed the strongest correlation (Fig. 7), where greater relative scour depth occurred in shallower waters, particularly at location with sediments composed of (63 \leq d_{50} < 200 μm) and medium sand (200 \leq d_{50} < 630 μm). In shallow waters the increased kinetic energy promotes stronger down-flow and vortex activity around the pile, enhancing scour, whereas in deeper water, hydrostatic pressure dominates, weakening these effects (Melville, 2008; FHWA, 2012), Furthermore, inclusion of the relative grain size captures the effect of grain-pile scaling, while the Keulegan-Carpenter number and the mobility parameter reflect the influence of flow unsteadiness and sediment mobility thresholds, reinforcing their relevance in realistic scour prediction frameworks.
- (2) Sediment-specific correlations: In order to explore the variability within soil classes, the data set was clustered according to d_{50} , and a PCA was applied to each cluster. For fine sand (63 to 200 μm) and medium sand (200 to 630 μm), relative water depth was found to be the dominant driver of relative scour depth, demonstrating the sensitivity of these sediment types to hydrodynamic forcing in shallower relative water depth. For coarser sediments, such as coarse sands (630 to 2000 μm) and fine gravels (2000 to 6300 μ m), the correlations were less pronounced, reflecting a greater resistance to scour. This sediment-specific analysis highlights the importance of considering sediment type when assessing scour susceptibility and designing OWFs, and how different sediment types can influence sediment transport patterns.
- (3) Site-specific variability: Due to local factors such as sediment conditions, hydrodynamic conditions, and topography, individual OWFs exhibited unique relative scour depth patterns. For example, London Array (Fig. 12C) showed correlations similar to the global results (Fig. 7), with relative water depth and site topography as the primary influences on scour, followed by current and wave conditions. In contrast, OWFs such as Robin Rigg and Lynn and Inner Dowsing showed no discernible correlations between relative scour depth and the key drivers obtained from the global PCA, highlighting the need for individual analyses to account for local complexities.

This study also highlights the potential environmental impacts of scour-induced sediment transport. While the primary focus was on identifying the physical drivers of scour, the findings could provide a first step in assessing potential impacts of OWF on the marine environment due to a changed regional sediment mobility. The entrainment of eroded sediment into the water column, with subsequent long-range transport, raises concerns about sediment deposition and potential impacts on benthic habitats and marine wildlife in far-field regions.

Future research should prioritize the refinement of predictive scour models that incorporate temporal data and expanded hydrodynamic parameters to improve accuracy in diverse sedimentary environments. In addition, integrated approaches that combine regional sediment transport modeling with ecological assessments are critical for evaluating the cumulative impacts of OWF facilities on marine ecosystems. These efforts will facilitate the development of sustainable OWF designs that minimize environmental disturbance while advancing renewable 821 energy goals.

- 822 Data availability: The data set used in this study is available in the Marine Data Exchange (MDE)
- 823 (https://www.marinedataexchange.co.uk/) and by the Copernicus Marine Service (CMEMS)
- 824 (https://marine.copernicus.eu/)

- 826 Authors contribution: K. G.: Writing original draft preparation, visualization, formal analysis,
- 827 conceptualization, methodology. C.J. Writing review & editing, supervision, conceptualization, project
- 828 administration. G.M. Writing review & editing, resources. A.S. Writing review & editing, methodology. M.W.
- 829 Writing review & editing, Supervision. T.S. Writing review & editing, Funding acquisition, Supervision.
- 830 Competing interests: The authors declare that they have no conflict of interest.
- 831 Acknowledgements: This work contributes to the DAM Research Mission sustainMare and the project
- 832 CoastalFutures (Project Number: 03F0911G) funded by the German Federal Ministry of Education and Research
- 833 (BMBF). The responsibility for the content of this publication lies with the authors.

834

835 References

- 836 Annad, M., Zourgui, N. H., Lefkir, A., Kibboua, A., and Annad, O.: Scour-dependent seismic fragility curves
- 837 considering soil-structure interaction and fuzzy damage clustering: A case study of an Algerian RC Bridge
- with shallow foundations, Ocean Engineering, 275, 114157, 2023.
- 839 Annad, M., Lefkir, A., Mammar-Kouadri, M., and Bettahar, I.: Development of a local scour prediction model
- clustered by soil class, Water Pract. Technol., 16, 1159–1172, 2021.
- 841 Baykal, C., Sumer, B. M., Fuhrman, D. R., Jacobsen, N. G., and Fredsøe, J.: Numerical investigation of flow and
- 842 scour around a vertical circular cylinder, Philos. Trans. R. Soc. A, 373, 20140104.
- 843 https://doi.org/10.1098/rsta.2014.0104, 2015.
- 844 Baelus, L., Bolle, A., and Szengel, V.: Long term scour monitoring around on a sandy seabed, in: Scour and
- 845 Erosion IX: Proceedings of the 9th International Conference on Scour and Erosion (ICSE 2018), November
- 5–8, 2018, Taipei, Taiwan, CRC Press, 2018.
- 847 Baeye, M., and Fettweis, M.: In situ observations of suspended particulate matter plumes at an offshore wind farm,
- 848 southern North Sea, Geo-Mar. Lett., 35, 247–255, 2015.
- 849 Bailey, H., Brookes, K. L., and Thompson, P. M.: Assessing environmental impacts of offshore wind farms:
- lessons learned and recommendations for the future, Aquat. Biosyst., 10, 1–13, https://doi.org/10.1186/2046-
- **851** 9063-10-8, 2014.
- 852 Bolle, A., De Winter, J., Goossens, W., Haerens, P., and Dewaele, G.: Scour monitoring around offshore jackets
- and gravity based foundations, in: Proceedings of the Sixth International Conference on Scour and Erosion,
- 854 Paris, France, 27–31, 2012.
- 855 Breusers, H. N. C., Nicollet, G., and Shen, H. W.: Local scour around cylindrical piers, J. Hydraul. Res., 15, 211-
- **856** 252, 1977.
- 857 Brignon, J. M., Lejart, M., Nexer, M., Michel, S., Quentric, A., Thiebaud, L.: A risk-based method to prioritize
- 858 cumulative impacts assessment on marine biodiversity and research policy for offshore wind farms in France,
- 859 Environ. Sci. Pol., 128, 264–276, https://doi.org/10.1016/j.envsci.2021.12.003, 2022.

- 860 Carpenter, J. R., Merckelbach, L., Callies, U., Clark, S., Gaslikova, L., and Baschek, B.: Potential impacts of
- 861 offshore wind farms on North Sea stratification, PLOS ONE, 11,
- https://doi.org/10.1371/journal.pone.0159512, 2016.
- 863 Carreiras, J., Larroudé, P., Seabra-Santos, F., and Mory, M.: Wave scour around piles, in: Coastal Engineering
- 864 2000, 1860–1870, 2001.
- 865 Chen, H., Zhang, J., Guo, Y., Cui, L., Guan, D., and Jiang, L.: Laboratory modelling study on the scour
- 866 characteristics around a jacket foundation subjected to combined wave-current loading, Renew. Energy,
- 867 122443, 2025.
- 868 Chiew, Y. M.: Local scour at bridge piers, Publication of: Auckland University, New Zealand, 1984.
- 869 Christiansen, N., Daewel, U., Djath, B., and Schrum, C.: Emergence of large-scale hydrodynamic structures due
- to atmospheric offshore wind farm wakes, Front. Mar. Sci., 64, https://doi.org/10.3389/fmars.2022.818501,
- **871** 2022.
- 872 CMEMS: Atlantic European North West Shelf Ocean Physics Reanalysis, https://doi.org/10.48670/moi-00059
- and 10.48670/moi-00060, 2023.
- 874 Corvaro, S., Mancinelli, A., and Brocchini, M.: Flow dynamics of waves propagating over different permeable
- beds, Coastal Engineering Proceedings, 35, 35–35, 2016.
- 876 COWRIE: A Further Review of Sediment Monitoring Data, Cowrie Ltd., Project reference ScourSed-09, 2010.
- 877 DECC: Dynamics of scour pits and scour protection Synthesis report and recommendations (Milestones 2 and
- 3), Department for Energy and Climate Change, Final Report, 2008.
- 879 Du, S., Wu, G., Zhu, D. Z., Wang, R., Lu, Y., and Liang, B.: Experimental study of local scour around submerged
- square piles in combined waves and current, Ocean Eng., 266, 113176, 2022.
- 881 Escarameia, M., and May, R. W. P.: Scour around structures in tidal flows, HR Wallingford, Wallingford, U.K.,
- **882** 1999.
- 883 EGS (International) Ltd.: Lynn and Inner Dowsing Offshore Wind Farms, Year 3 Post-Construction Survey
- 884 (2011), Phase 1 Geophysical Survey, Job No. 4918, Final Report Rev 7, CREL Reference No LD-O-EV-
- 885 013-0000-000000-368-D, Marine Data Exchange, https://www.marinedataexchange.co.uk/details/TCE-
- 886 1041/2011-egs-lynn-and-inner-dowsing-year-3-post-construction-survey-phase-1---geophysical-
- survey/summary, 2012.
- 888 EGS (International) Ltd.: Lynn and Inner Dowsing Offshore Wind Farms (October 2012), Job No. 5038, Final
- Report Rev1, Marine Data Exchange, https://www.marinedataexchange.co.uk/details/TCE-1076/2012-egs-
- 890 lynn-and-inner-dowsing-offshore-wind-farms-post-construction-hydrographic-and-geophysical-
- survey/summary, 2013.
- 892 EU: An EU Strategy to harness the potential of offshore renewable energy for a climate-neutral future, European
- 893 Commission, Communication COM/2020/741 final, 2020.
- 894 Federal Highway Administration (FHWA): Evaluating scour at bridges (HEC-18, Publication No. FHWA-HIF-
- 895 12-003), U.S. Department of Transportation, 2012.
- 896 Gabriel, K. R.: The Biplot Graphic Display of Matrices with Application to Principal Component Analysis,
- Biometrika, 58, 453–467, https://doi.org/10.1093/biomet/58.3.453, 1971.
- 898 Gazi, A. H., Purkayastha, S., and Afzal, M. S.: The equilibrium scour depth around a pier under the action of
- collinear waves and current, J. Mar. Sci. Eng., 8, 36, 2020.

- 900 Guşatu, L. F., Menegon, S., Depellegrin, D., Zuidema, C., Faaij, A., and Yamu, C.: Spatial and temporal analysis
- 901 of cumulative environmental effects of offshore wind farms in the North Sea basin, Sci. Rep., 11, 1-18,
- 902 https://doi.org/10.1038/s41598-021-89537-1, 2021.
- 903 Harasti, A., Gilja, G., Adžaga, N., and Škreb, K. A.: Principal Component Analysis in development of empirical
- 904 scour formulae, in: Proceedings of the 7th IAHR Europe Congress, Athens, Greece, 7–9 September 2022,
- 905 271–272, 2022.
- 906 Harris, J. M., Herman, W. M., and Cooper, B. S.: Offshore windfarms: an approach to scour assessment, in: Y. M.
- 907 Chiew, S.-Y. Lim, and N.-S. Cheng (Eds.), Proceedings of the 2nd International Conference on Scour and
- 908 Erosion, Stallion Press, Singapore, 283–291, 2004.
- 909 Harris, J. M., Tavouktsoglou, N. S., Couldrey, A., Whitehouse, R. J., and Klapper, J.: Scour prediction in cohesive
- 910 marine soils: a hybrid approach, ISSMGE Int. J. Geoeng. Case Histories, 7, 59–75, 2023.
- 911 Harris, J., and Whitehouse, R. J. S.: Scour prediction in non-uniform soils: Undrained shear strength and
- 912 erodibility, 2014.
- 913 Hancu, S.: Sur le calcul des affouillements locaux dans la zone des piles de ponts, in: Proceedings of the 14th
- 914 IAHR Congress, 299–313, 1971.
- 915 Hu, R., Wang, X., Liu, H., and Lu, Y.: Experimental study of local scour around tripod foundation in combined
- 916 collinear waves-current conditions, Journal of Marine Science and Engineering, 9(12), 1373, 2021.
- 917 Jolliffe, I. T., and Cadima, J.: Principal component analysis: a review and recent developments, Philosophical
- 918 Transactions of the Royal Society A: Mathematical, Physical and Engineering Sciences, 374(2065),
- 919 20150202, 2016.
- 920 Kenyon, N., and Cooper, B.: Sand banks, sand transport and offshore wind farms, Gov. British, 2005.
- 921 Laursen, E. M.: An analysis of relief bridge scour, J. Hydraul. Div., Proc. ASCE, 89(HY3), 93–118, 1963.
- 922 Link, O., and Zanke, U.: On the time-dependent scour-hole volume evolution at a circular pier in uniform coarse
- 923 sand, in: Proc. 2nd International Conference on Scour and Erosion (ICSE), 2004.
- 924 Lloret, J., Turiel, A., Solé, J., Berdalet, E., Sabatés, A., Olivares, A., Gili, J.-M., Vila-Subirós, J., and Sardá, R.:
- 925 Unravelling the ecological impacts of large-scale offshore wind farms in the Mediterranean Sea, Sci. Total
- 926 Environ., 824, 153803, 2022.
- 927 Louwersheimer, W. F., Verhagen, H. J., and Olthof, J.: Scour around an offshore wind turbine, in: Coastal
- 928 Structures 2007 Proceedings of the 5th Coastal Structures International Conference, CST07, Venice, Italy,
- 929 1903–1912, 2009.
- 930 London Array Ltd.: Environmental Statement Volume 1: Offshore Works, Technical report, London Array Ltd.,
- 931 2005.
- 932 Lyu, X., Cheng, Y., Wang, W., An, H., and Li, Y.: Experimental study on local scour around submerged monopile
- under combined waves and current, Ocean Eng., 240, 109929, 2021.
- 934 May, R. P., and Willoughby, I. R.: Local scour around large obstructions, HR Wallingford Report SR240, 1990.
- 935 Matutano, C., Negro, V., López-Gutiérrez, J.-S., and Esteban, M. D.: Scour prediction and scour protections in
- 936 offshore wind farms, Renew. Energy, 57, 358–365, 2013.
- 937 Matthieu J., Raaijmakers T. Interaction between Offshore Pipelines and Migrating Sand Waves. 2012.
- 938 McGovern, D. J., Ilic, S., Folkard, A. M., McLelland, S. J., and Murphy, B. J.: Time development of scour around
- a cylinder in simulated tidal currents, J. Hydraul. Eng., 140(6), 04014014, 2014.
- 940 Melling, G. J.: Hydrodynamic and geotechnical controls of scour around offshore monopiles, University of
- Southampton, Ocean and Earth Science, Doctoral Thesis, 250 pp., 2015.

- 942 Melville, B.: The physics of local scour at bridge piers, in: Proceedings of the 4th International Conference on
- 943 Scour and Erosion, 28–38, 2008.
- 944 Noormets, R., Ernstsen, V., Bartholoma, A., Flemming, B., and Hebbeln, D.: Local scour in a tidal environment:
- a case study from the Otzumer Balje tidal inlet, southern North Sea, Poster reproduced in Appendix A of
- 946 Offshore Center Danmark, 2006, 2003.
- 947 Qi, W. G., and Gao, F. P.: Physical modeling of local scour development around a large-diameter monopile in
- combined waves and current, Coast. Eng., 83, 72–81, 2014.
- 949 Qi, M., Li, J., and Chen, Q.: Comparison of existing equations for local scour at bridge piers: parameter influence
- 950 and validation, Nat. Hazards, 82, 2089–2105, 2016.
- 951 Qu, L., An, H., Draper, S., Watson, P., Zhao, M., Harris, J., Whitehouse, R., and Zhang, D.: A review of scour
- impacting monopiles for offshore wind, Ocean Engineering, 301, 117385, 2024.
- 954 Richardson, M. D., Valent, P., Briggs, K., Bradley, J., and Griffin, S.: NRL mine burial experiments, in:
- Proceedings of the 2nd Australian-American Joint Conference on the Technologies of Mines and Mine
- 956 Countermeasures, Sydney, Australia, 1–23, 2001.
- 957 Rivier, A., Bennis, A. C., Pinon, G., Magar, V., and Gross, M.: Parameterization of wind turbine impacts on
- hydrodynamics and sediment transport, Ocean Dyn., 66, 1285–1299, 2016.
- 959 Roulund, A., Sutherland, J., Todd, D., and Sterner, J.: Parametric equations for Shields parameter and wave orbital
- 960 velocity in combined current and irregular waves, 2016
- 961 Rudolph, D., Bos, K. J., Luijendijk, A. P., Rietema, K., and Out, J. M. M.: Scour around offshore structures -
- Analysis of field measurements, in: Y. M. Chiew, S.-Y. Lim, and N.-S. Cheng (Eds.), Proceedings of the 2nd
- 963 International Conference on Scour and Erosion, Stallion Press, Singapore, 400–407, 2004.
- 964 Saathoff, J. E., Goldau, N., Achmus, M., Schendel, A., Welzel, M., and Schlurmann, T.: Influence of scour and
- 965 scour protection on the stiffness of monopile foundations in sand, Appl. Ocean Res., 144, 103920, 2024.
- 966 Sarkar, A.: Scour and flow around submerged structures, in: Proceedings of the Institution of Civil Engineers-
- Water Management, 167(2), 65–78, Thomas Telford Ltd., February 2014.
- 968 Sarmiento, J., Guanche, R., Losada, I. J., Rosendo, E. M., Guindo, A., and de Guevara, J. L.: Scour processes
- around pile clusters of jacket foundations under steady currents, Ocean Eng., 313, 119502, 2024.
- 970 Schendel, A.: Wave-current-induced scouring processes and protection by widely graded material, Leibniz
- University Hannover, Dissertation, https://doi.org/10.15488/4453, 2018.
- 972 Schendel, A., Welzel, M., Schlurmann, T., and Hsu, T.-W.: Scour around a monopile induced by directionally
- 973 spread irregular waves in combination with oblique currents, Coast. Eng., 161, 103751,
- 974 https://doi.org/10.1016/j.coastaleng.2020.103751, 2020.
- 975 Schultze, L. K. P., Merckelbach, L. M., Horstmann, J., Raasch, S., and Carpenter, J. R.: Increased mixing and
- 976 turbulence in the wake of offshore wind farm foundations, J. Geophys. Res. Oceans, 125(8), e2019JC015858,
- 977 2020.

- 978 Sheppard, D. M., Odeh, M., and Glasser, T.: Large scale clear-water local pier scour experiments, J. Hydraul.
- 979 Eng., 130(10), 957–963, 2004.
- 980 Shields, M. A., Woolf, D. K., Grist, E. P., Kerr, S. A., Jackson, A. C., Harris, R. E., and Side, J.: Marine renewable
- 981 energy: The ecological implications of altering the hydrodynamics of the marine environment, Ocean Coast.
- 982 Manag., 54(1), 2–9, 2011.

- 983 Sheppard, D. M., Zhao, G., and Ontowirjo, B.: Local scour near single piles in steady currents, in: Water Resources 984 Engineering, pp. 1809–1813, ASCE, 1995.
- Sheppard, D. M., Ontowirjo, B., and Zhao, G.: Conditions of Maximum Local Scour, in: Proceedings of Stream
 Stability and Scour at Highway Bridges, Resources Engineering Conference 1991–1998, edited by
 Richardson, E. V., and Lagasse, P. F., ASCE, Reston, VA, 1999.
- 990 Smith, J. D., and McLean, S. R.: Spatially averaged flow over a wavy surface, J. Geophys. Res., 82(12), 1735–991 1746, 1977.
- Soulsby, R. L., and Whitehouse, R. J. S.: Threshold of sediment motion in coastal environments, in: Pacific Coasts
 and Ports '97: Proceedings of the 13th Australasian Coastal and Ocean Engineering Conference and the 6th
 Australasian Port and Harbour Conference, Vol. 1, pp. 145–150, Centre for Advanced Engineering, University
 of Canterbury, Christchurch, NZ, 1997.
- 996 Soulsby, R.: Dynamics of Marine Sands, Thomas Telford Ltd., 1997.
- 997 Stahlmann, A.: Numerical and experimental modeling of scour at foundation structures for offshore wind turbines, 998 in: ISOPE International Ocean and Polar, June 2013.
- 999 Sturt, F., Dix, J. K., and EMU Ltd.: The Outer Thames Estuary Regional Environmental Characterisation, Marine
- Aggregate Levy Sustainability Fund, 09/J/1/06/1305/0870, Technical report, Marine Aggregate Levy
- Sustainability Fund, 2009.

- Sumer, B. M., Fredsøe, J., and Christiansen, N.: Scour around vertical pile in waves, J. Waterway Port Coastal
 Ocean Eng., 118, 15, 1992.
- Sumer, B. M., and Fredsøe, J.: Scour around pile in combined waves and current, J. Hydraul. Eng., 127(5), 403–1005 411, 2001.
- Sumer, B. M., Petersen, T. U., Locatelli, L., Fredsøe, J., Musumeci, R. E., and Foti, E.: Backfilling of a scour hole around a pile in waves and current, J. Waterway, Port, Coastal, Ocean Eng., 139(1), 9–23, 2013.
- 1008 Teilmann, J., and Carstensen, J.: Negative long term effects on harbour porpoises from a large scale offshore wind
- farm in the Baltic evidence of slow recovery, Environ. Res. Lett., 7, https://doi.org/10.1088/1748 9326/7/4/045101, 2012.
- 1011 Van Rijn, L. C.: Sediment transport, part I: bed load transport, J. Hydraul. Eng., 110(10), 1431–1456, 1984.
- $1012 \quad Vanhellemont, \, Q., \, and \, Ruddick, \, K.: \, Turbid \, wakes \, associated \, with \, offshore \, wind \, turbines \, observed \, with \, Landsat \, Contract and \, Contract are consistent and a contract are contract. \\$
- 1013 8, Remote Sens. Environ., 145, 105–115, 2014.
- 1014 Walker, W.: Field measurements of local pier scour in a tidal inlet, MSc, University of Florida, 1995.
- 1015 Watson, S. C., Somerfield, P. J., Lemasson, A. J., Knights, A. M., Edwards-Jones, A., Nunes, J., and Beaumont,
- N. J.: The global impact of offshore wind farms on ecosystem services, Ocean Coast. Manag., 249, 107023,
- 1017 https://doi.org/10.1016/j.ocecoaman.2024.107023, 2024.
- 1018 Welzel, M., Schendel, A., Schlurmann, T., and Hildebrandt, A.: Volume-based assessment of erosion patterns
- around a hydrodynamic transparent offshore structure, Energies, 12(16), 3089, 2019.
- 1020 Welzel, M.: Wave-current-induced scouring processes around complex offshore structures, 2021.
- 1021 Welzel, M., Schendel, A., Satari, R., Neuweiler, I., and Schlurmann, T.: Spatio-temporal analysis of scour around
- 1022 complex offshore foundations under clear water and live bed conditions, Ocean Eng., 298, 117042, 2024.
- 1023 Wilson, J. C., and Elliott, M.: The habitat-creation potential of offshore wind farms, Wind Energy, 12(2), 203-
- 1024 212, 2009.
- 1025 Whitehouse, R.: Dynamics of estuarine muds. Thomas Telford, 2000.
- 1026 Whitehouse, R. J. S., Harris, J. M., Mundon, T. R., and Sutherland, J.: Scour at offshore structures, in: Proceedings
- of the 5th International Conference on Scour and Erosion, San Francisco, 11–20, 2010.

- 1028 Whitehouse, R. J. S., Harris, J. M., Sutherland, J., and Rees, J.: The nature of scour development and scour
- protection at onshore wind farm foundations, Mar. Pollut. Bull., 62(1), 73–88, 2011.
- 1030 Whitehouse, R. J. S., and Harris, J.: Scour prediction offshore and soil erosion testing, HR Wallingford Report,
- 1031 2014
- 1032 Yao, Y., Chen, Y., Zhou, H., and Yang, H.: Numerical modeling of current loads on a net cage considering fluid-
- structure interaction, J. Fluids Struct., 62, 350–366, 2016.
- 1034 Zhao, M., Zhu, X., Cheng, L., and Teng, B.: Experimental study of local scour around subsea caissons in steady
- 1035 currents, Coast. Eng., 60, 30–40, 2012.
- 1036 Zanke, U. C. E., Hsu, T.-W., Roland, A., Link, O., and Diab, R.: Equilibrium scour depths around piles in
- noncohesive sediments under currents and waves, Coastal Eng., 58(10), 986–991, 2011.
- 1038